Resistance Element Welding (REW) of Steels with Non-Ferrous Materials: Potentials, Challenges, and Properties

metals

MDPI

Review

Resistance Element Welding (REW) of Steels with Non-Ferrous Materials: Potentials, Challenges, and Properties

Mohammad Abankar [1], Manuela De Maddis [1,2], Valentino Razza [1,2] and Pasquale Russo Spena [1,2,*]

[1] Department of Management and Production Engineering, Politecnico di Torino, Corso Duca degli Abruzzi 24, 10129 Torino, Italy; mohammad.abankar@polito.it (M.A.); manuela.demaddis@polito.it (M.D.M.); valentino.razza@polito.it (V.R.)

[2] Advanced Joining Technologies Center (J-Tech@PoliTO), Politecnico di Torino, Corso Duca degli Abruzzi 24, 10129 Torino, Italy

* Correspondence: pasquale.russospena@polito.it

Abstract: Performance and functionality are two key factors in designing advanced components. One promising approach in manufacturing design is the fabrication of multi-material structures by joining dissimilar materials. Steels, known for their outstanding properties and cost-effective production, are widely used across several industries. However, their high density presents challenges when designing lightweight components. A solution lies in combining steels with lightweight, non-ferrous alloys to develop cost-effective multi-material parts. However, joining different materials is generally complex due to their different properties, making it sometimes challenging or even unfeasible. Resistance element welding (REW) offers a high-performance alternative to traditional methods, such as resistance spot welding, with a high potential in mass production industries like automotive manufacturing. This article comprehensively reviews the latest research on REW for dissimilar joining of steels and non-ferrous alloys. It focuses on the microstructural and mechanical properties of joints, innovations in the REW process, the influence of process parameters on joint quality, as well as simulation and numerical studies. In addition, REW is compared with traditional joining methods.

Keywords: resistance element welding; dissimilar joining; mechanical properties; microstructure

Citation: Abankar, M.; De Maddis, M.; Razza, V.; Russo Spena, P. Resistance Element Welding (REW) of Steels with Non-Ferrous Materials: Potentials, Challenges, and Properties. *Metals* **2024**, *14*, 1448. https://doi.org/10.3390/met14121448

Academic Editor: Masahiro Fukumoto

Received: 28 October 2024
Revised: 9 December 2024
Accepted: 10 December 2024
Published: 17 December 2024

1. Introduction

Reducing energy consumption and mitigating greenhouse gas emissions are crucial objectives for the automotive industry, particularly as environmental regulations become more stringent [1,2]. European authorities, for example, have mandated a 30% reduction in emissions by 2030 compared to 2020 levels. Since fossil fuels are a major contributor to greenhouse gas emissions, car manufacturers play a pivotal role in achieving these targets. Key strategies to reduce emissions include vehicle weight reduction, enhancing engine efficiency, decreasing CO_2 emissions from fuel use, and developing hybrid systems [3]. A 10% reduction in vehicle weight, for instance, can result in a 5.5% decrease in fuel consumption [3,4].

Steels remain the most widely used materials in the automotive industry due to their cost-effectiveness and excellent properties. Advanced High Strength Steels (AHSSs), such as boron and Dual-Phase (DP) steels, are commonly used because of their high specific strength [5–7]. However, the demand for materials with even higher strength-to-weight ratios has driven interest in lightweight alternatives such as composites, hybrid materials, and non-ferrous alloys [5,8–10]. For instance, aluminum alloys can lower vehicle weight by up to 50% compared to steel without compromising safety or structural integrity [5]. Recent research has focused on developing multi-material structures that combine non-ferrous materials with steel to further decrease component weight. These structures aim to exploit the hybrid properties of different materials to achieve superior performance [6,11–16]. This lightweight design approach is increasingly adopted in mass automotive production

and other industries to reduce greenhouse gas emissions and improve fuel efficiency [17]. Materials used for these components must exhibit good formability for vehicle design and adequate weldability for effective joining. Promising candidates for the next generation of vehicles include fiber-reinforced composites, magnesium, aluminum, and titanium alloys. For example, magnesium alloys offer high specific strength, good shock absorption, and castability [18–21]. Titanium alloys are known for their outstanding specific strength, fracture toughness, and corrosion resistance, making them suitable for automotive and aerospace applications [22–25]. Aluminum alloys are appreciated for their low density, high corrosion resistance, machinability, recyclability, and cost-effectiveness in large-scale production [26].

Despite the advantages of multi-material structures, achieving reliable joints between dissimilar materials remains a significant challenge for engineers and researchers. Currently, resistance spot welding (RSW) is the leading joining technique used in the automotive industry (Figure 1), with an estimated 3000 to 7000 spot welds in a typical vehicle [14]. RSW involves welding two or more metal sheets by applying pressure and heat generated by an electric current at the weld area. Once the material melts, the current is switched off, and the electrode pressure is maintained until the molten nugget solidifies, forming the joint. RSW is a cost-effective, automatic, fast, and reliable welding technology [27–31]. However, while it is well-suited for joining similar metal grades (e.g., steel to steel, aluminum to aluminum), joining dissimilar metals (e.g., steel to aluminum) poses some issues in producing high-quality joints. These challenges arise mainly from differences in thermal expansion, conductivity, melting temperature, and mechanical properties, as well as chemical incompatibilities between metals in their molten state. For example, aluminum alloys typically have two to three times the thermal conductivity of steel grades, requiring a welding current nearly three times higher. In addition, RSW welding of aluminum to steel forms a sort of weld-brazing joint, as the welding temperature exceeds the melting point of aluminum but is below that of steel [32]. Moreover, brittle intermetallic compounds (Fe_xAl_y) between aluminum and iron notably decrease joint mechanical strength and ductility.

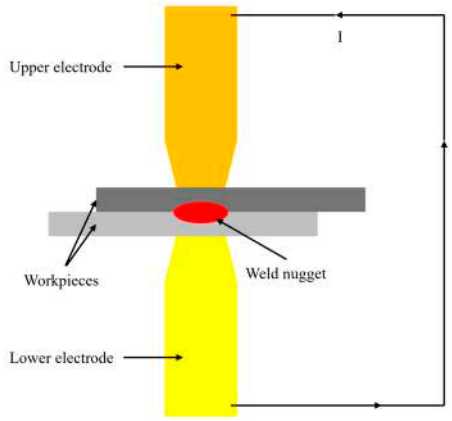

Figure 1. Schematic illustration of a RSW process (I: Intensity of current).

To address these challenges, several welding technologies have been proposed for vehicle component assembly, even though some of these technologies cannot meet industrial requirements. For example, friction stir spot welding (FSSW), a solid-state joining technology competing with RSW [33] for welding dissimilar materials, is often unsuitable due to the high cost and complexity of the equipment. In addition, the remaining keyhole is undesirable as it can serve as a site for corrosion and stress concentration [34]. To address this issue, refill friction spot welding (RFSSW) was developed by GKSS-GmbH [34]. However, this technique cannot be easily integrated into existing welding systems, especially in mass-production environments. Cold metal transfer spot plug welding [35] is inefficient for mass production because of its low throughput. Similarly, mechanical joining through

self-piercing riveting (SPR) [36] remains a challenge when joining AHSSs and ultra-high-strength steels (UHSSs). This cold-forming technique fastens two or more sheets using a rivet, but when the materials have excessive strength and low formability, the rivet fails to penetrate the sheet stack, leading to weak interlocking, insufficient penetration, and cracks [37]. In addition, SPR is limited by the range of sheet thickness it can accommodate [11]. Clinching, another joining method used in the automotive industry, is generally used to join non-load-bearing structures, as its joints are not as resistant as those produced by RSW or SPR. In addition, clinching, which involves the local deformation of metal parts, shares similar limitations to SPR in joining high-strength materials [38–40]. Ultrasonic spot welding offers improved joint strength, but its use is restricted to thin or soft sheets because of the low power output of ultrasonic equipment [41].

A more recent technology, resistance element welding (REW), has been developed to overcome the above-mentioned limitations in joining dissimilar materials. REW integrates mechanical fastening (riveting) with thermal joining (welding), creating a hybrid fusion process. This method is particularly effective for joining materials that are difficult to weld and chemically incompatible, such as steel to aluminum, sandwich, polymers, and composites [37]. In the REW process, a steel rivet is first inserted into the upper layer, followed by a welding operation, similar to RSW, at the interface between the steel and the rivet [16]. Studies [12,16,42,43] comparing the mechanical properties of RSW and REW joints indicate that REW joints generally exhibit superior mechanical performance, such as higher tensile strength, even with lower welding currents. For example, Ling et al. [6] demonstrated that REW joints between UHSS 22MnMoB and aluminum 6061 alloys achieved a peak load of 7086.9 N and an energy absorption of 11.38 J at a low welding current of 9 kA. In contrast, RSW joints using a higher welding current of 16 kA only reached a peak load of 957 N and absorbed 0.09 J. The steel nugget formed in REW replaces the brittle intermetallic compound (IMC) layer, significantly enhancing load-bearing capacity. Similarly, Manladan et al. [16] reported that REW joints between AZ31 magnesium alloy and 316L steel achieved a peak load of 3.71 kN and energy absorption of 10.2 J, compared to 2.3 kN and 1.14 J for RSW joints. Energy absorption (i.e., failure energy), that is, the energy absorbed by a weld for failure, is crucial for vehicle crashworthiness and is determined by calculating the area under the load–displacement curve up to the maximum load point [43]. Figure 2 illustrates the tensile shear strength from Al/steel joints obtained with four different competing joining technologies—RSW, REW, SPR, and FSSW—based on data from the literature [5,6,12,26,36,44–61]. Although these studies can cover different Al/steel combinations, the findings consistently show that RSW exhibits relatively low tensile shear load values, mostly ranging between 2–4 kN. This indicates that RSW provides the lowest mechanical strength among the compared welding technologies. This is primarily attributed to the well-known chemical incompatibility between iron and aluminum in the molten state. This incompatibility promotes the formation of significant amounts of Al/Fe IMCs, which adversely affect joint strength. In contrast, REW and SPR exhibit improved tensile shear strength, generally ranging from 4–8 kN, making them more suitable for applications requiring higher mechanical performance. FSSW demonstrates a moderate tensile shear load performance, with values typically ranging between 3–6 kN, partially overlapping with those of REW and SPR. This suggests that while FSSW can be a competitive alternative in certain scenarios, it does not consistently achieve the strength levels provided by REW and SPR.

The limitations of many technologies in joining dissimilar materials have prompted growing interest in REW as a promising alternative. One of the key advantages of REW is its compatibility with RSW infrastructure, allowing manufacturers to use their existing equipment with minimal additional investment, which is particularly beneficial for high-volume production. REW is well-suited for producing outer panels (e.g., side panels and roofs using thin aluminum sheets on steel structures), panel components (e.g., floor parts and front walls made of aluminum and steel), and structural parts (e.g., C- and D-pillars, crash reinforcements, and instrument panel supports). As an example, Figure 3 shows the

advantage of REW over SPR in joining certain car parts in the body-in-white of the Audi A6 C8. SPR either fails or is severely limited, while REW successfully improves joint quality and reliability in these areas.

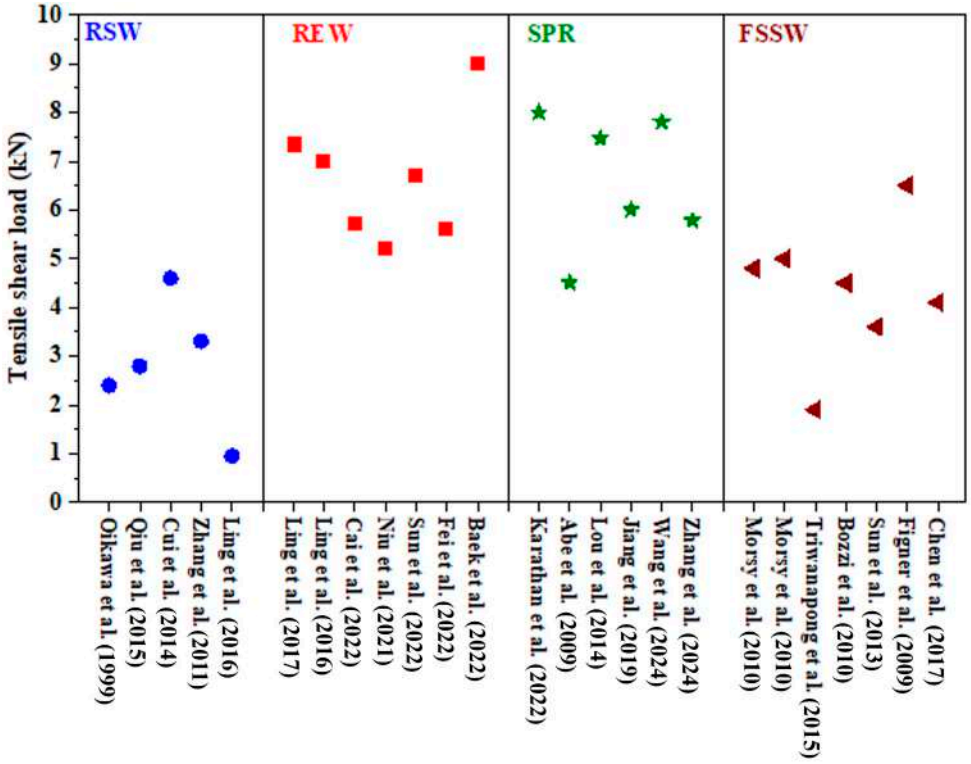

Figure 2. A comparison of the tensile-shear load performance of RSW, REW, SPR, and FSSW Al/steel joints. Adapted from Refs. [5,6,12,26,36,44–61].

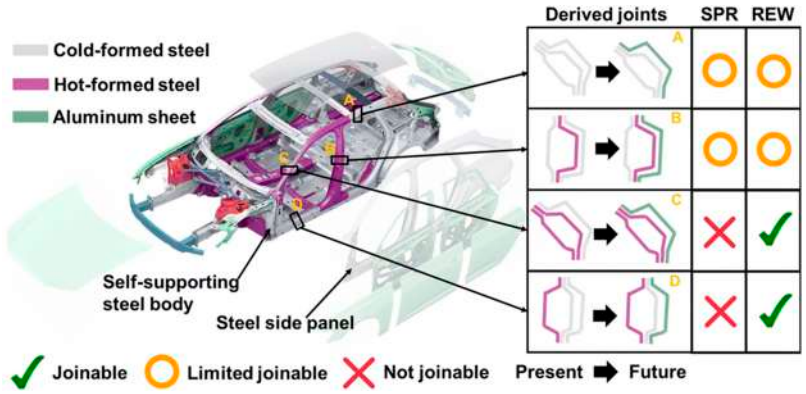

Figure 3. Self-supporting steel body of the Audi A6 C8 using a steel side panel and the feasibility of SPR and REW for selected joints. Reprinted from Ref. [62].

REW demonstrates superior capability in joining dissimilar materials, such as non-ferrous to ferrous alloys, which is challenging to obtain through traditional RSW. REW is particularly effective for metallurgically incompatible light alloy/steel combinations [37], offering reliable joints with improved quality and minimal distortion through the use of a rivet—a third element facilitating the welding process [6]. This makes REW highly beneficial for lightweight multi-material structures in the automotive and aerospace industries, where durability, efficiency, and safety are critical [12,16,42,43]. Unlike the competing RSW, which can subject materials to excessive heat input, REW ensures controlled heat applica-

tion, preserving part geometry and tolerances, making it a superior choice for spot-joining heat-sensitive components [37].

This review aims to provide a comprehensive study of the recent advancements and methodologies in resistance element welding, addressing the growing importance of this technique as an efficient and effective solution for joining dissimilar materials. Previous studies have focused on individual experimental results but lack an overall perspective. This work fills this gap by summarizing the latest advancements, methodologies, and research trends in REW while highlighting challenges, opportunities, and key directions for future innovation.

2. Fundamentals of REW

Meschut et al. [63] first introduced REW as a joining method for car body parts. As illustrated in Figure 4, the REW process differs from conventional RSW since it uses a rivet-like resistance element, compatible with the bottom sheet, as the auxiliary joining part. In the first stage of the process (Figure 4a), the rivet is punched into the upper material (generally a non-ferrous sheet). The shaped punch facilitates a force-and-form-locking connection between the upper sheet and the rivet, ensuring that the rivet remains securely in place and preventing its dislodgment [37]. In the second stage, two water-cooled electrodes are placed on either side of the overlapping sheets, applying pressure to ensure intimate contact. A welding current is then applied, generating heat due to the electrical resistance of the sheets (i.e., Joule's effect), forming a molten nugget. Once the current is stopped, the nugget cools under continuous pressure from the electrodes, creating a metallurgical bond between the rivet and the lower sheet. Therefore, the REW process is a hybrid joining technique that combines both thermal (metallurgical bonding) and mechanical (locking and force-fit) methods [11]. REW can be performed in two configurations: pre-assembled and self-punching. In the pre-assembled method, the process consists of two distinct stages—punching and welding—conducted separately, as shown in Figure 4. In contrast, the self-punching method integrates both punching and welding in a single step. While the pre-assembled method offers easier handling, it is more time-consuming due to its two-stage nature. On the other hand, the self-punching method is faster but can be more complex to execute. Niu et al. [64] proposed a novel self-punching method called resistance rivet welding (RRW) and evaluated its performance when joining aluminum and press-hardened steel. They performed the RRW process using a traditional RSW welding machine in four steps: 1. Positioning—the rivet is pre-pressed onto the upper sheet by the two electrodes to ensure proper alignment; 2. Thermal piercing—the electrode applies pressure to the rivet and while a heating current, I_1, is circulating, the rivet is pushed down until it contacts the surface of the bottom sheet; 3. Welding current application—a second current, I_2, similar to that used in RSW, is applied; meanwhile, the aluminum extruded from the upper sheet gradually fills the grooves in the rivet; 4. Retreating step—the electrodes are slightly withdrawn, completing the formation of the final nugget. The study reported a joint strength of 481 MPa for the Al/steel RRW joint, approximately 100 MPa higher than the strength of the Al/steel REW joint previously investigated by Ling et al. [5]. This enhanced strength was attributed to the larger nugget size and reduced softening of the aluminum sheet in the RRW process compared to REW.

Since the main stage of the REW process is identical to RSW, a thorough understanding of RSW principles is essential for comprehending the REW process.

Figure 4 shows the main types of electrical resistance involved during the final welding stage of REW: contact resistance at the electrode/rivet interface (R1), bulk resistance of the sheets (R2 and R4), resistance at the faying interface (R3), electrode/bottom sheet interface (R5), and rivet/upper sheet resistance (R6). In addition, the resistances of the upper and lower electrodes are denoted as R_U and R_L, respectively. The total electrical resistance in the REW process for a certain alloy is the sum of all these individual resistances [65]. Ideally, R_U and R_L should remain low since the primary function of electrodes is to generate electrical current across the sheets. R3 plays a pivotal role, as it directly affects nugget

formation at the faying interface. If R3 is too low, nugget formation may fail; conversely, if R3 is too high, it can result in improper heat generation and excessive melting [66]. Heat generation in the second stage of the REW technology is based on Joule's law [67]:

$$Q = R\, I^2\, t \quad (1)$$

where Q [J] is the heating input, I [A] the welding current, R [Ω] the electrical resistance of the sheet stack, and t [s] the welding time. Thus, the heat generated during the REW process increases with higher current, longer welding duration, and greater electrical resistance.

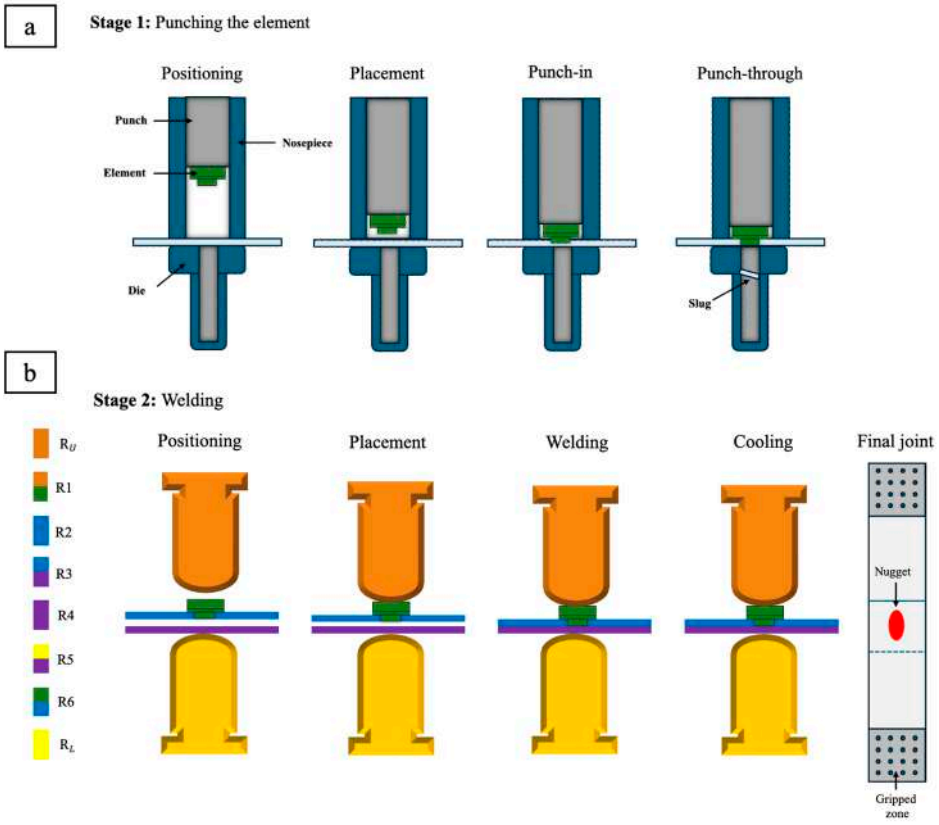

Figure 4. Illustration of the principles of REW: (**a**) stage of punching an element; (**b**) stage of welding.

3. Welding Parameters in REW Technique

Welding current is the main factor influencing joint quality in RSW and REW, and it must be controlled within an optimal range. A lower welding current produces a smaller nugget, which decreases the tensile shear load of joints [68–70]. On the other hand, an excessive welding current leads to poor joint quality and severe expulsion of molten metal [57,68,71]. Cai et al. [12] studied the REW joining of aluminum alloy and steel, finding that excessive welding current from 18 kA to 22 kA reduced the joint area in an aluminum plate from 32.8 mm^2 to 29.5 mm^2 and decreased the load-bearing capacity from 5712 N to 5440 N, respectively. Moreover, increasing the welding currents from 12 kA to 22 kA lowered the hardness of the heat-affected zone (HAZ) in the aluminum plate from 78 HV to 66 HV, which reduced the shear tension load and caused necking and failure within the aluminum HAZ. Meschut et al. [72] recommended that for optimal joint strength, the nugget diameter should be at least 50% of the shaft diameter of the weld rivet. While welding time also influences heat input (according to Equation (1)), the welding current has a more significant impact due to its exponential relationship with heat generation. Generally, as welding time increases, so do heat input and nugget size; however, prolonged welding time can lead to issues such as electrode degradation [71]

and coarsening of the fusion zone (FZ) and HAZ microstructures, which adversely affect hardness and strength [68].

Figure 5 displays the effect of welding current on peak load, energy absorption, and nugget diameter in the joining of AZ31 magnesium alloy and 316 austenitic stainless steel (ASS) [16]. The results show that as the welding current increased from 5 to 8 kA, energy absorption and peak load increased from 2.85 to 10.19 J and 1.85 to 3.71 kN, corresponding with an increase in nugget diameter. However, further increasing the current to 9 kA decreased peak load and energy absorption to 2.75 kN and 3.5 J despite the slightly larger nugget diameter. This drop was attributed to the melting of the magnesium alloy around the rivet, which widened the rivet hole and reduced joint quality [16]. Qiu et al. [59] also observed that in REW of steel and aluminum, both sheets around the rivet were welded together, similar to dissimilar RSW. As the welding current increased from 21 to 23 kA, the joint area widened, but metal expulsion occurred at too high currents, and joint strength decreased from 3.85 to 3.3 kN. This reduction was attributed to overheating of the aluminum alloy, which led to a reduction in thickness, thereby weakening the joint.

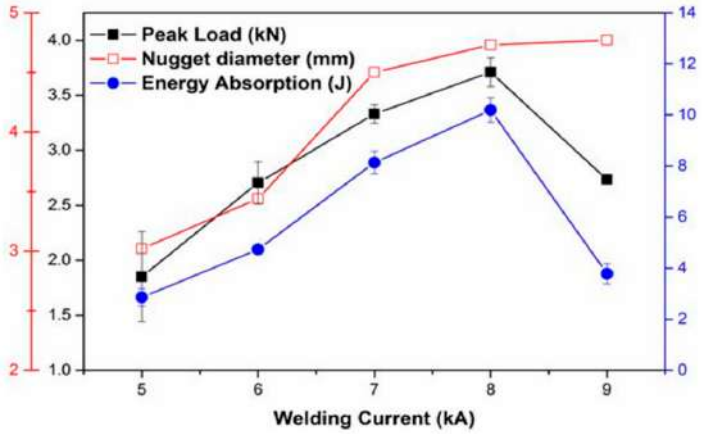

Figure 5. Effect of welding current on the nugget diameter, peak load, and energy absorption of AZ31 magnesium alloy and 316 ASS joints produced by REW. Reprinted from Ref. [16].

Electrode force is another key parameter in the REW process, although it plays a less critical role than in RSW. In RSW, the presence of oxide layers on aluminum or magnesium alloys makes the process highly sensitive, requiring high electrode force to break through the oxide layer and reduce the high contact resistance it creates [73,74]. If left unaddressed, these oxide layers degrade overall weld quality [75,76]. Since the oxide layer is adherent, refractory, and non-conducting, it also accelerates electrode degradation. Therefore, the oxide layer should be removed, although this process can be time-consuming and costly [77]. In addition, excessive electrode force in RSW can cause sheet separation and increased electrode wear [3,68]. In REW, the electrode force primarily secures the steel rivet against the bottom plate, thus mitigating issues related to oxide layers. However, maintaining a balanced electrode force is still essential for optimal performance.

Meinhardt et al. [78] conducted an experimental study on the role of different auxiliary joining elements in REW in joint strength. They found that REW joints made with cold-forged rivets exhibited higher shear strength than the conventional REW process, likely due to the enhanced locking and force-fit. In another study, Wang et al. [79] used a rivet with a larger diameter (8 mm instead of 6 mm) and observed an increased peak load from 11.5 to 13.8 kN and energy absorption from 24 to 28 J. However, this approach contradicts the industrial goal of reducing weight. Cai et al. [12] integrated a concealed riveting cover in the REW joining of DP780 steel and aluminum 5052 to obtain a flat and smooth workpiece surface, thereby enhancing the joint's resistance to collision-induced damage.

4. Nugget Formation During REW

Several experimental and numerical studies have investigated nugget formation in the REW of aluminum alloys [6,16]. Sun et al. [26] described the heating process in REW as occurring in multiple stages. Initially, heat is generated at the faying interface due to the high resistance between the rivet and DP600 steel. As the process continues, this heat causes the melting and joining of the two steel sheets under electrode force, forming and enlarging the nugget. Although larger nugget sizes are generally associated with enhanced mechanical properties in both RSW and REW joints, excessive nugget growth in the thickness direction can negatively affect joint performance [26]. Conversely, insufficient heat input results in smaller nugget sizes, reducing the contact area between the sheets and, subsequently, weakening the joint's mechanical properties [12,13,80]. Ling et al. [6] studied nugget formation in REW when joining boron steel and aluminum 6061 alloy. They found that contact and bulk resistance mainly influence the heat generated by Joule's effect. As shown in Figure 6, no melting was observed at 20 ms on either the aluminum or steel sides. According to Figure 6f, bulk resistance increased at the beginning of the welding process until the contact surface of boron steel and aluminum 6061 started melting, initiating nugget formation. As the nugget formed, electrical conductivity within the molten nugget increased, reducing electrical resistance. By 100 ms, aluminum near the rivet started melting due to heat conduction from the nugget. Since aluminum alloy has a higher thermal conductivity than the rivet, heat was rapidly transferred from the rivet to the aluminum 6061 alloy, concentrating more heat on the boron steel side. As a result, the nugget shifted toward the steel. This shifting phenomenon was similarly observed in REW joints between aluminum 6061-T6 and DP780 steel, owing to the higher thermal conductivity of aluminum 6061-T6 compared to DP780 [5].

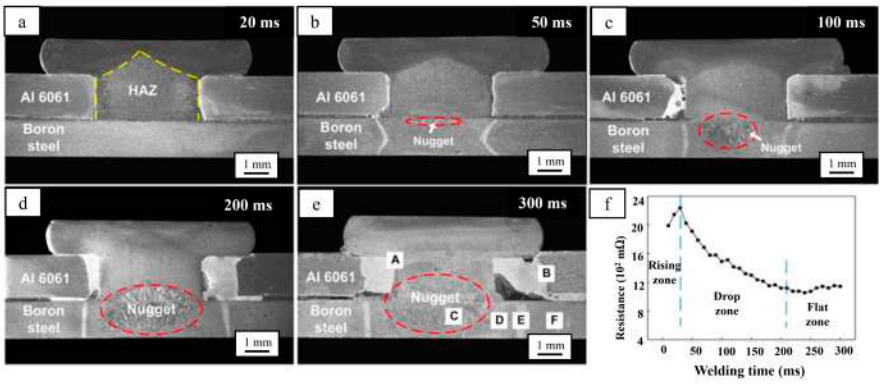

Figure 6. (**a**–**e**) Nugget formation and growth and (**f**) dynamic resistance of 9 kA REW. Reprinted with permission from Ref. [6]. Copyright 2024 Taylor & Francis.

Manladan et al. [42] investigated the REW joining of a magnesium alloy and stainless steel, both with and without adhesive. Their findings revealed that, at the same welding current, the nugget diameter in resistance element weld-bonding (REWB) joints was slightly larger than in standard REW joints. This difference was attributed to the adhesive, which enhanced the contact resistance between the sheets, thereby enhancing Joule heating at the faying interface [42]. Duric et al. [43] studied nugget formation in REW joints of aluminum alloy and DP500 steel. They found that a significant portion of the nugget with a martensitic microstructure formed within the Q235 steel rivet. The asymmetrical nugget shape was attributed to differences in thermal conductivity and electrical resistivity between the rivet and DP500 steel. Similarly, Fei et al. [60] also reported an asymmetrical nugget in the REW joining of aluminum alloy and Q235 rivet. In this case, the asymmetry was attributed to differences in the thickness of the Q235 rivet (2 mm) and the bottom sheet (1.5 mm). The greater thermal mass of the rivet generated more heat on the rivet side, contributing to the asymmetrical nugget formation. In another study, Manladan et al. [81] investigated nugget formation in a three-sheet REW configuration of magnesium alloy/ASS/ASS. As shown in

Figure 7, macrostructures of joints welded with a current range of 5–10 kA exhibited an asymmetrical nugget at all welding currents, with the nugget size at the ASS/ASS interface larger than that at the rivet/ASS interface. The larger nugget at the ASS/ASS interface was attributed to the fact that the electrical resistance of ASS is 6 to 8 times higher than that of the low-carbon steel rivet. Despite the nugget shifting, joint strength remained unaffected. However, at excessive welding currents, as shown in Figure 7g, pores formed in the center of the nugget, and the rivet hole widened, reducing joint quality.

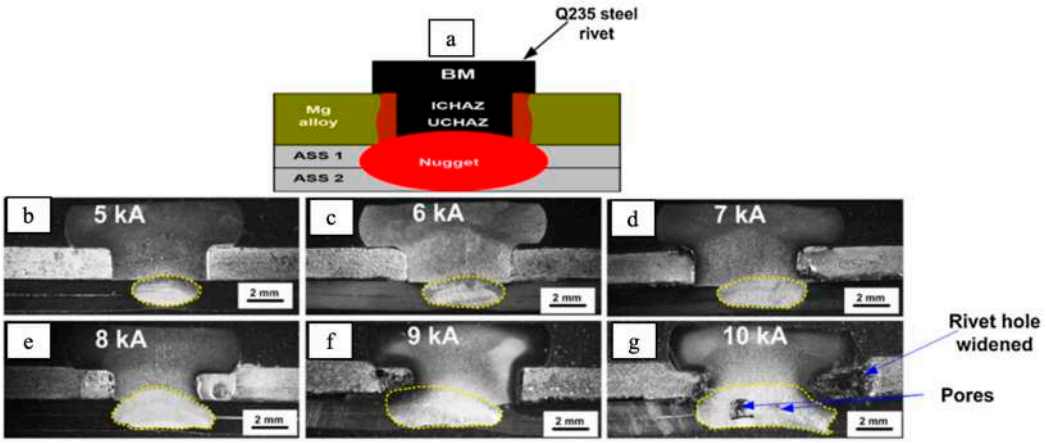

Figure 7. (**a**) Schematic diagram of the REW joints; (**b**–**g**) macrostructures of the joints at different welding currents. Reprinted with permission from Ref. [81]. Copyright 2024 Elsevier.

Cai et al. [12] studied the REW joining of DP780 steel and aluminum alloy using a concealed rivet. As shown in Figure 8, the nugget formed predominantly on the DP780 steel side, while the molten aluminum near the rivet was extruded at the interface of the two sheets. This local extrusion reduced the load-bearing capacity of the aluminum sheet due to the significant decrease in joint thickness. The joint was divided into several distinct regions: Region A is the transition zone of the aluminum alloy, including the FZ and HAZ. Region B is the inter-critical HAZ (ICHAZ), Region C is the upper-critical HAZ (UCHAZ), and Region D is the nugget zone. The following sections provide a detailed analysis of these regions.

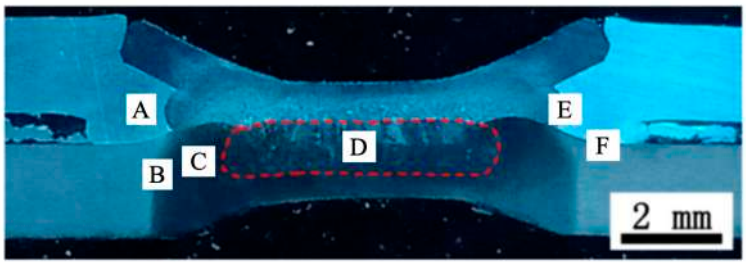

Figure 8. Optical microscopy image of the REW joint. Reprinted from Ref. [12].

5. Macrostructure and Microstructure of REW Joints

The thermal gradient within the weld and the chemical composition of the base alloy are two critical factors that notably influence the weld microstructure [82,83]. Since most alloys and rivet materials used in the REW process are steel, determining the carbon equivalent (CE) index is essential for understanding microstructural evolution during joining. The CE index can be calculated using the formula (chemical elements in %wt.) provided by AWS D1.1 [84]:

$$CE = C + 1/6\ Mn + 1/5\ (Cr + Mo + V) + 1/15\ (Ni + Cu) + 1/6\ Si \quad (2)$$

A higher CE value corresponds to a lower weldability and increased hardness in steel. Ling et al. [5] studied the REW joining of aluminum alloy and DP steel, reporting that the HAZ in the DP steel exhibited greater hardness than the HAZ of the rivet, which they attributed to the higher CE value of the steel. Niu et al. [61] investigated the REW process in Al/steel joints and calculated the CE values of both the rivet and bottom steel sheets to predict the microstructure evolution in the weld and rivet. Using CE values (from 0.23 to 0.38), along with the Fe-C phase diagram [85], they mapped the solidification and phase transformation path of the nugget, as shown in Figure 9. The solidification/transformation process follows this sequence:

$$Liq \rightarrow Liq + \delta \rightarrow Liq + \gamma \rightarrow \gamma \rightarrow Martensite$$

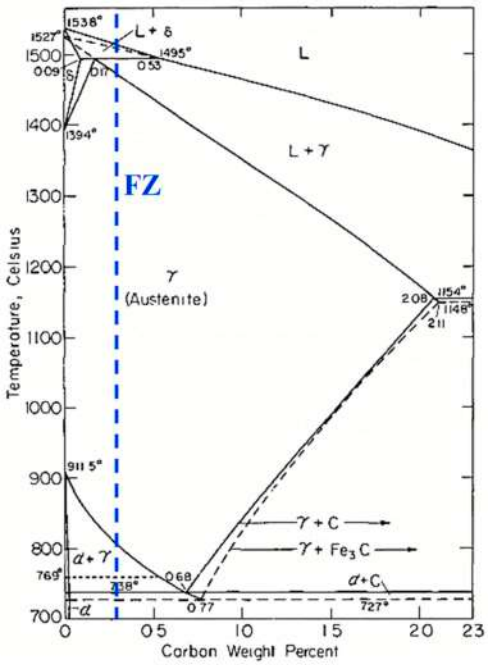

Figure 9. Fe-C phase diagram. Reprinted with permission from Ref. [61]. Copyright 2024 Elsevier.

These transformations suggest that the peak temperature occurs within the FZ, followed by the rapid solidification of the molten nugget. Initially, high-temperature ferrite is formed, which then rapidly transforms into γ-austenite during the peritectic reaction. Finally, the austenite completely transformed into lath martensite due to the high cooling rate.

The following sub-sections provide a detailed discussion of the microstructure and macrostructure of different joint regions, including the HAZ, nugget, and the interface between the upper sheet and rivet, as well as the upper and bottom sheets, as depicted in Figure 10.

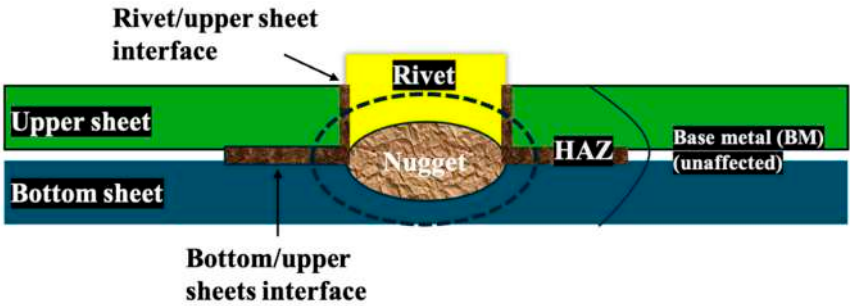

Figure 10. Schematic cross-section of a REW weld.

5.1. Microstructure of the Nugget

In the REW joining of steel with other materials, steel is commonly selected for both the bottom sheet and the rivet. However, the specific type of steel can vary, leading to differences in properties that significantly affect nugget formation and the microstructure. This variation arises from the distinct electrical resistances of different steel grades, which influence the heat input during the welding process. For example, Figure 11a shows an asymmetrical nugget formed between a Q235 rivet and 316 ASS in an REW joint [16]. Due to the greater electrical resistance of the Q235 rivet, a significant portion of the nugget (denoted as FZ2) forms on the Q235 side, while a peripheral FZ (FZ1) forms on the ASS side. The differences in heat input and cooling rates between these materials contribute to the different microstructures within the nugget. Figure 11c,d shows the microstructures of FZ1 and FZ2, respectively. The nugget on the ASS side contains more delta ferrite than the one on the Q235 side, as it experienced a higher cooling rate due to its proximity to the water-cooled electrode.

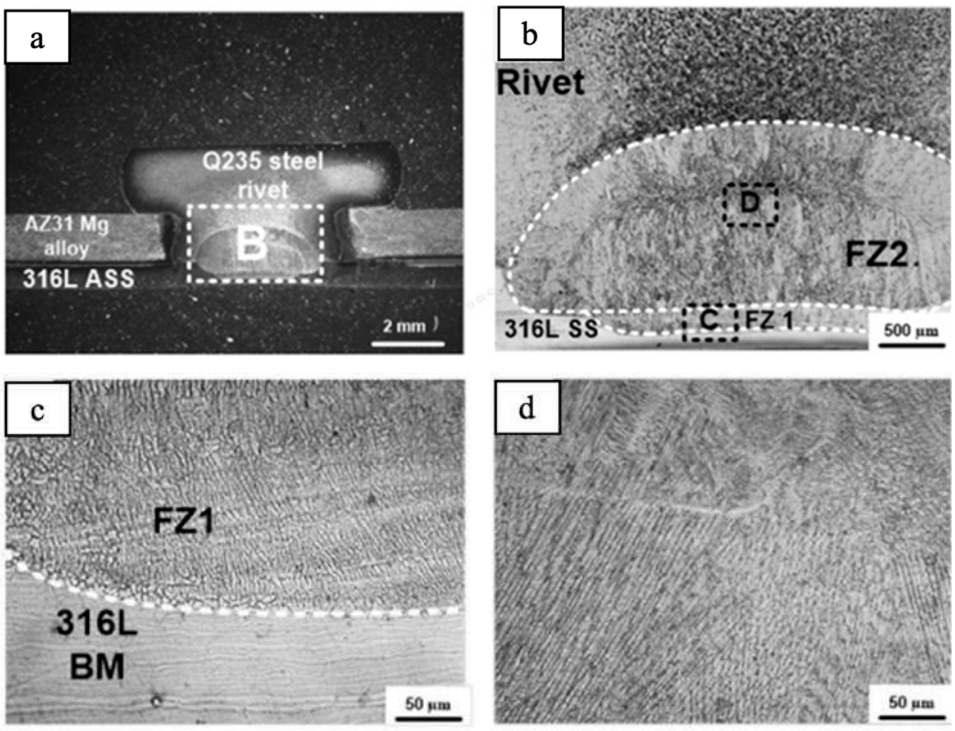

Figure 11. Macrostructure and microstructure of the REW joint of AZ31 magnesium alloy and 316 L ASS: (**a**) macrostructure of REW joint, (**b**) magnified region B in (**a**), (**c**) microstructure of region C in (**b**), and (**d**) microstructure of region D in (**b**). Reprinted from Ref. [16].

Ling et al. [6] studied the REW joining of boron steel and aluminum, reporting the formation of coarse and consistent lath martensite as a result of the high hardenability of boron steel. They also reported [5] that a nugget consisting of large lath martensite formed during the REW process between DP780 steel and aluminum 6061-T6 alloy, which was attributed to the high cooling rate experienced after welding. The steel nugget exhibited an as-cast feature due to the remelting of this region during welding. In addition, most of the steel nuggets formed in the bottom sheet, since the aluminum upper sheet acted as a cooling medium owing to its higher thermal conductivity. Similarly, Fei et al. [60] also observed lath martensite in the nugget of Al/steel REW joints, consistent with the role of high cooling rates in the formation of such hard and brittle microstructures in the weld zone.

Sun et al. [26] investigated the effect of an external magnetic field on the porosity and microstructure evolution in DP600/AA6061 REW joints. Their research revealed that the assistance of electromagnetic stirring increased the nugget size between the Q235 rivet and DP600 steel, as shown in Figure 12. The redistribution of heat led to grain refinement within the weld nugget. In the REW joints without the external magnetic field, coarse pores were observed at low welding currents, while finer pores appeared at higher welding currents. The introduction of the magnetic field disrupted the dendritic structure and effectively eliminated pores within the nugget. Furthermore, the HAZ width was reduced in joints subjected to the external magnetic field compared to conventional REW joints. Overall, the magnetically assisted REW (MA-REW) joints exhibited a 10.2% increase in tensile-shear load and a 26.8% increase in fracture displacement during tensile testing, indicating an improvement in mechanical performance compared to conventional REW joints.

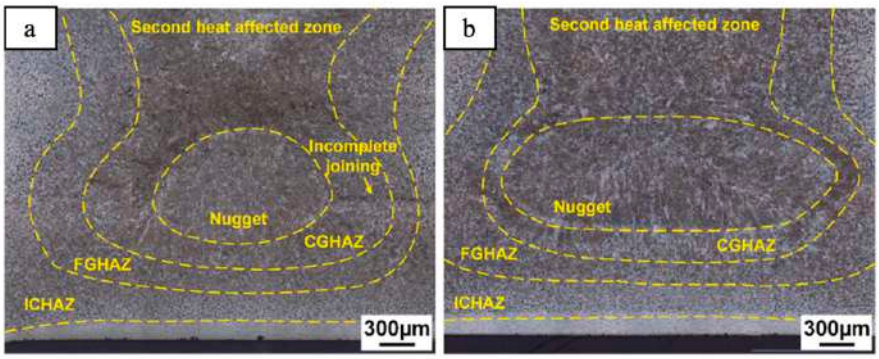

Figure 12. Cross-sectional morphologies of REW and MA-REW joints with the distribution of HAZ: (**a**) REW; (**b**) MA-REW. Reprinted with permission from Ref. [26]. Copyright 2024 Elsevier.

5.2. Microstructure of the Upper Sheet

In the REW process, the connection between the rivet and bottom sheet can be considered similar welding, while the connection between the rivet and the upper sheet remains a dissimilar welding scenario. Ling et al. [5] studied the REW joining of DP780 steel and 6061-T6 aluminum alloy, observing the formation of a uniform 4 μm thick IMC layer between the bottom and upper sheets, as well as a less consistent 3 μm thick IMC layer at the rivet/upper sheet interface. These IMCs are a result of the near-zero solubility between steel and aluminum [5]. Figure 13 shows the microstructures of regions A to F, as identified in Figure 6e [6]. Region A, which corresponds to the rivet/Al alloy interface, displays a clear intermetallic layer formed during the final welding stage of the REW process. This phase promotes diffusion between the molten aluminum and steel, leading to the solidification of a FeAl IMC from α-Fe [59]. The scanning line in Figure 13g confirms the presence of a 4 μm thick Fe-Al IMC layer at the rivet/Al alloy interface [6]. Qiu et al. [59] also investigated the REW joining of steel with aluminum alloy and identified a similar 4 μm FeAl intermetallic layer at the rivet/Al interface, along with FeAl3 at the steel/aluminum alloy interface. Interestingly, the formation of IMCs at the aluminum/rivet interface is not necessarily detrimental in REW joints [6]. While IMC layers can reduce the mechanical properties in traditional RSW joints, their presence in REW joints suggests proper contact between the aluminum and the rivet. In addition, the significant difference in thermal expansion coefficients between aluminum alloy (around 23.6×10^{-6} K^{-1}) and steel rivet (around 11.75×10^{-6} K^{-1}) [59], combined with electrode force, helps maintain contact between the two materials. These differences in thermal expansion and diffusion facilitate material locking through IMC formation. Cai et al. [12] also studied the REW joining of aluminum and steel, confirming the presence of a $FeAl_3$ IMC layer between the rivet and aluminum sheet, consistent with Qiu et al. [59]. These studies suggest that while a thin IMC layer can increase joint strength, an excessively thick layer may lead to crack nucleation and propagation through the IMC, compromising joint integrity.

Ling et al. [6] further noted that during the REW process, the aluminum upper sheet near the steel rivet tends to melt due to its higher heat conductivity and lower melting point than steel. The presence of dendritic structures in the aluminum microstructures is evidence of aluminum melting during welding [61]. Region B in Figure 13 represents the transition zone between the base material (BM) and the FZ of the aluminum alloy. Fei et al. [60] reported aluminum brazing around the rivet and steel plate, indicating that the high thermal conductivity of aluminum alloys causes most of the heat generated at the Al/steel interface to transfer to the aluminum side, leading to melting near the rivet. As depicted in Figure 14, the nugget forms predominantly on the aluminum side, featuring columnar grains aligned in the direction of heat diffusion.

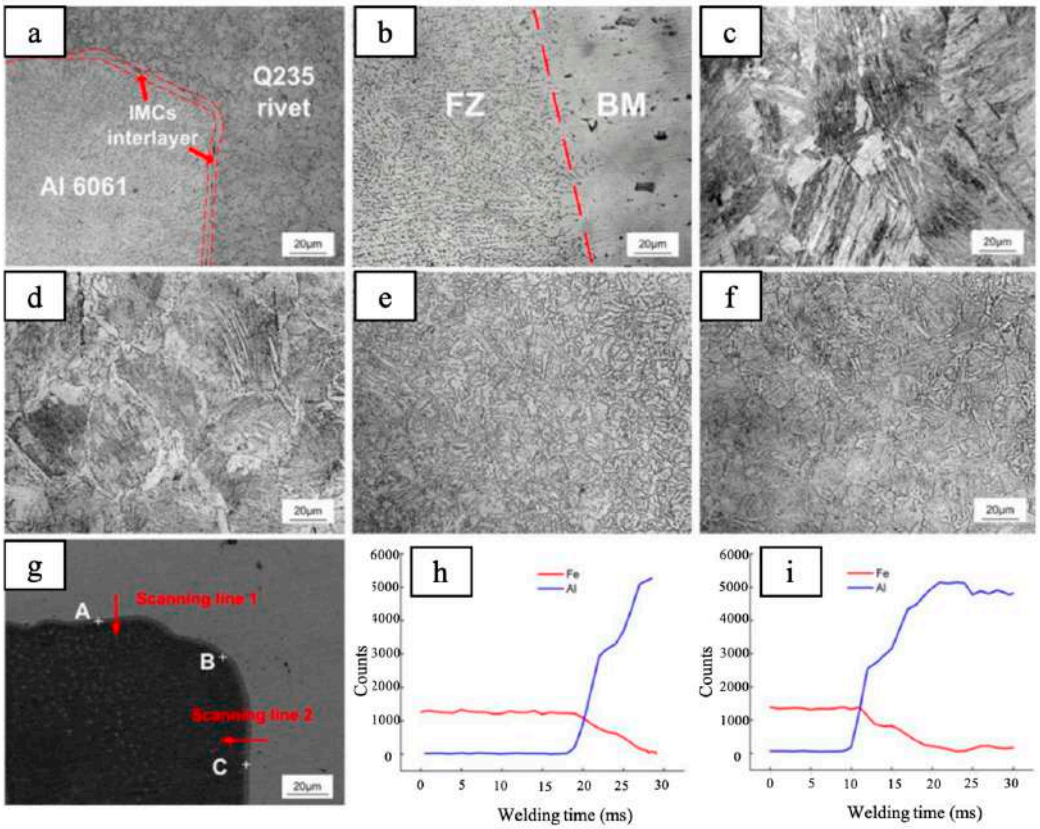

Figure 13. (**a**–**f**) Microstructure image of (**a**–**f**) regions in Figure 6e, (**h**) scanning line 1 and (**i**) scanning line 2 in (**g**). Reprinted with permission from Ref. [6]. Copyright 2024 Taylor & Francis.

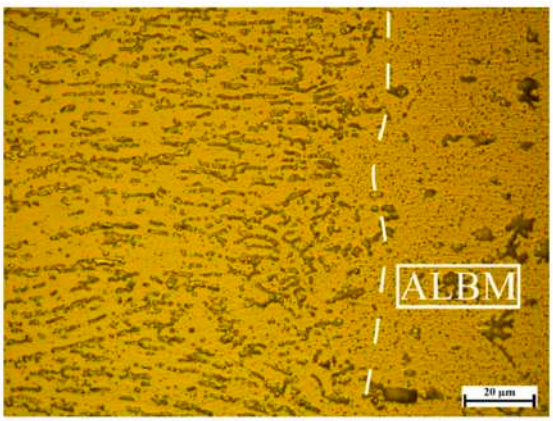

Figure 14. Aluminum nugget in the FREW joint. Reprinted with permission from Ref. [60]. Copyright 2024 Springer Nature.

5.3. Microstructure of the HAZ

The peak temperature and cooling rate are key factors influencing the formation of different microstructures in the HAZ of REW joints. The HAZ microstructure in steel can vary significantly depending on these factors. Ling et al. [6] and Manladan et al. [16] categorized the HAZ into two main regions: the UCHAZ and ICHAZ. The UCHAZ experienced temperatures higher than the A_{C3} transformation temperature but below the melting point, while the ICHAZ experienced temperatures between A_{C1} and A_{C3}. Ling et al. [6] examined the microstructure in the HAZ during the REW of 6061 aluminum and boron steel. As shown in Figure 13d, Region D corresponds to the UCHAZ, where coarse, featherlike bainite forms due to the temperature being above A_{C3} but below the melting point. In contrast, Region E represents the ICHAZ, containing a mix of fine acicular ferrite and pearlite. Figure 13f illustrates a region similar to the BM, where the peak temperature remained below A_{C1}. Manladan et al. [16] studied the microstructural characteristics of the HAZ in the REW joint of 316 L ASS and AZ31 magnesium alloy with a Q235 rivet. They observed that the UCHAZ experienced peak temperatures above A_{C3}, leading to a complete transformation of austenite into martensite due to the high cooling rate. In contrast, the ICHAZ contained a mixture of austenite and ferrite, which transformed into pearlite during final cooling. As a result, the ICHAZ exhibited a combination of ferrite and pearlite, with a higher pearlite content compared to the BM, attributed to the austenitic transformation.

Ling et al. [5] also investigated the HAZ formed during the REW joining of DP780 steel and 6061-T6 aluminum alloy. The HAZ in the DP780 steel was divided into three regions: coarse-grained HAZ (UCHAZ with coarse lath martensite), fine-grained HAZ (UCHAZ with fine lath martensite), and ICHAZ. The coarse-grained HAZ was subjected to temperatures remarkably above A_{C3}, resulting in the formation of larger lath martensite, while the fine-grained HAZ experienced slightly lower temperatures, above A_{C3}, producing finer lath martensite. The UCHAZ closer to the FZ exhibited coarser grains because of the higher temperature achieved, whereas finer grains formed in regions with lower peak temperatures [60].

Fei et al. [60] investigated the REW joint of aluminum and Q235 alloys and found that, in the ICHAZ, only part of the microstructure transformed into austenite, while the remainder became allotriomorphic ferrite. The grain size in the coarse-grained HAZ was smaller compared to the nugget, and incomplete austenitization in the ICHAZ led to partial martensitic transformation, resulting in higher martensite content than the DP780 BM. In addition, the grain size progressively decreased with increasing distance from the nugget. Ling et al. [5] introduced an additional HAZ region near the BM, positioned between the BM and the ICHAZ. This region, termed subcritical HAZ, is the softest region due to its peak temperature remaining below A_{C1}. In this area, the martensite undergoes tempering, leading to a reduction in hardness.

5.4. Microstructure in the Three Sheets Configuration

Manladan et al. [81] investigated the REW joining of a magnesium alloy and two types of stainless steel. They demonstrated that the microstructure of the weld nugget can be divided into different regions based on varying microstructural features. The formation of equiaxed grains at the nugget center was attributed to a lower G/R ratio, where G is the temperature gradient and R is the solidification growth rate. A reduced G/R ratio increases constitutional supercooling, which promotes the columnar-to-equiaxed transition (CET). As depicted in Figure 15, the nugget center exhibited equiaxed dendritic grains (EDG), a result of the lower temperature gradient in this region (Figure 15c). In contrast, the edges of the nugget, particularly in the rivet and the bottom stainless steel sheet, displayed a columnar dendritic grain (CDG) structure, as shown in Figure 15b,d. The columnar grains at the edge of the nugget in the bottom stainless steel sheet were finer than those at the rivet edge, which can be attributed to the lower cooling rate experienced by the rivet compared to the bottom ASS. The microstructure of the magnesium alloy, Figure 15e, revealed columnar

dendritic grains, indicating that the magnesium near the rivet had melted and subsequently resolidified during the welding process.

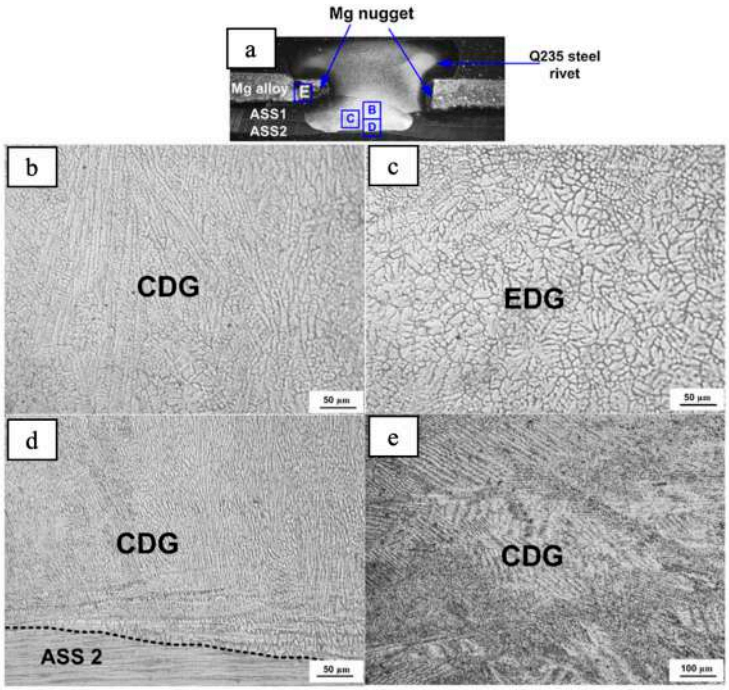

Figure 15. Typical macrostructure of the REW joints; (**b**–**e**) microstructures of the corresponding regions in (**a**). Reprinted with permission from Ref. [81]. Copyright 2024 Elsevier.

6. Hardness of REW Joints

The formation of different microstructures due to varying thermal histories during the REW process leads to distinct hardness profiles across the welded joint. Even within the rivet, the hardness can vary significantly depending on the thermal history. Ling et al. [6], in their study on the REW joining of DP780 steel and aluminum 6061, found that the hardness at the top of the rivet was higher than that of the rivet base material. They attributed this hardness increase to the strain hardening caused by the electrode punching. When different types of steel are used for the rivet and bottom sheet, variations in the nugget hardness can occur. One critical factor influencing these variations is the carbon equivalent index of steel, with the steel having a lower carbon equivalent typically exhibiting lower hardness in the nugget during REW [86]. In addition, different phase transformations in materials contribute to hardness differences within REW joints.

Manladan et al. [16] examined the REW of AZ31 magnesium alloy and 316 ASS. They divided the nugget into two regions: the main nugget and the peripheral nugget. The main nugget experienced martensitic transformation, resulting in a higher hardness of around 401.3 HV, compared to 331.5 HV in the periphery nugget. They also measured the hardness values of the UCHAZ, ICHAZ, and BM, which were 427, 282, and 244 HV, respectively. The UCHAZ showed the highest hardness due to its faster cooling rate, leading to an increased martensite content.

Ling et al. [6] further investigated the hardness profile in REW joints between boron steel and aluminum 6061. They observed that the nugget exhibited the highest hardness, around 450 HV, primarily due to the presence of martensite. The HAZ zone was divided into two different regions: one containing coarse, feather-like bainite (hardness of 400 HV) and another containing fine acicular ferrite and pearlite (hardness of 270 HV), as shown in Figure 13d,e. The melted aluminum near the rivet had a hardness of 70 HV, lower than the BM hardness of 101 HV, leading to failure within the aluminum alloy during tensile testing. In another study, Ling et al. [5] studied the hardness behavior of the REW joint between DP780 steel and 6061-T6 aluminum alloys. They identified the subcritical HAZ in

DP780 steel as the softest region, with a hardness of around 200 HV, attributed to tempered martensite. The softest region in the Q235 rivet was found in the BM, with a hardness of 185 HV. The aluminum side had the softest region with a hardness of 83 HV, resulting from remelting and recrystallizing during the welding process.

Niu et al. [61] examined the microhardness of REW joints between aluminum 6061 T-6 and stainless steel. As shown in Figure 16, they divided the aluminum side of the joint into four zones based on microhardness distribution: base material (BM), transition zone (TZ), softening zone (SZ), and re-solidified zone (RZ). The reduction in hardness, particularly in the softening zone, was primarily caused by the coarsening and dissolution of precipitates. The RZ near the rivet exhibited higher hardness than the SZ, attributed to the formation of Fe-rich strengthening phases. According to Pouranvari et al. [87], the SZ in the upper sheet is a critical region, since it governs the failure location of REW joints. Ling et al. [6] also reported that during the REW process, the aluminum sheet displayed a soft region with lower hardness than the BM, leading to a base-metal fracture mode. Failure typically occurred within the aluminum sheet, as it had lower hardness than both the joint and the steel sheet [6].

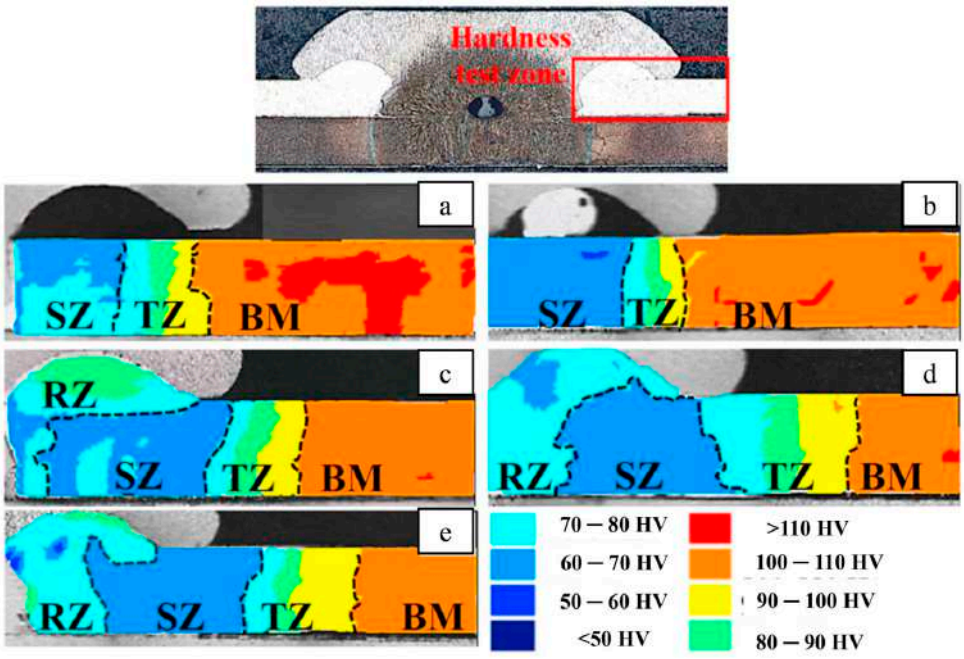

Figure 16. Hardness profiles at different welding currents: (**a**) 5 kA, (**b**) 6 kA, (**c**) 7 kA, (**d**) 8 kA, and (**e**) 9 kA. Reprinted with permission from Ref. [61]. Copyright 2024 Elsevier.

7. The Role of Adhesive Bonding on the REW Joints

Adhesive bonding (AB) is widely used across several industries and is often combined with other joining processes, such as RSW and REW, to increase mechanical properties and corrosion resistance [68,88]. In joints involving dissimilar alloys like aluminum and steel, which have a significant difference in electrochemical potential (−1.62 V), corrosion resistance can be compromised [72]. The application of an adhesive layer acts as an insulating barrier between these materials, effectively preventing galvanic corrosion [16]. Moreover, the adhesive layer reduces noise, harshness, and vibration, improving the overall performance of the joint [89].

Meschut et al. [72] investigated the REW and friction element welding (FEW) processes for joining an aluminum alloy and steel (with and without a zinc coating). Several studies have focused on joining aluminum alloy to hot-dipped zinc-coated steel [5,90–92]. Arghavani et al. [93] found that the melting and evaporation of the coating layer can reduce its thickness, thereby decreasing joint quality. They measured the thickness of the coating layer before and after the FEW and REW and found that while coating degradation

occurred in the FEW joints, no damage was observed in the REW joints. To evaluate the effectiveness of fastener coatings against saline electrolytes, both coated and uncoated samples were subjected to cathodic electrodeposition dip painting, a process commonly used in the automotive industry for corrosion protection. The results showed that fasteners with a zinc-nickel coating exhibited no corrosion products during testing. Only white rust (zinc oxide) with crystalline salt appeared on the joint surface, indicating that the coating effectively prevented red rust (iron oxide). Therefore, the zinc-nickel coating maintained its corrosion resistance even after the joining process.

AB considerably affects the mechanical properties of REW joints. During welding, the decomposition of adhesives enriches the welding regions with carbon, leading to higher hardness than conventional REW [42,94]. Holtschke and Jüttner [37] reported that using an adhesive layer in REW reduced the required welding current compared to non-adhesive conditions. However, if the welding current is too low, the adhesive layer can act as insulation, hindering the welding process. Manladan et al. [42] investigated the influence of an adhesive layer at the interface between magnesium alloy and ASS joined via REW and RSW. They found that AB resulted in higher peak load and elongation at fracture in resistance element weld-bonding (REWB) and resistance spot weld-bonding (RSWB) joints compared to conventional REW and RSW joints. In addition, REWB joints showed superior peak load and energy absorption compared to RSWB joints. This improvement was attributed to the penetration of carbon atoms from the adhesive, which increased hardness in both REWB and RSWB joints. Moreover, REWB joints exhibited approximately twice the peak load and six times the energy absorption of conventional REW joints, primarily due to the increased nugget diameter caused by the adhesive bond. The adhesive increases contact resistance at the faying interface, thus enhancing Joule heating. Fei et al. [94] investigated the joining of aluminum alloy and steel using flat resistance element welding bonding (FREWB). FREWB joints exhibited a higher peak load and larger nugget sizes than FREW. However, the brittleness of the adhesive layer led to lower energy absorption in FREWB joints compared to FREW joints. In FREWB joints, the load is distributed across two regions: the welding zone (WZ) and the adhesive bond zone (ABZ). When the FREWB joint reached its peak load, the ABZ failed first, causing a sudden drop in tensile-shear load. While AB offers benefits, using it alone can lead to issues such as creep, low strength under peel loads, and extended curing times [63]. However, combining adhesive bonds with RSW significantly improves joint strength [95]. Schemal and Meschut [96] examined the welding lobe of REW joints between LITECOR^{TM} (sandwiches with steel cover layers) and steel, with and without adhesive. As shown in Figure 17, their findings revealed that using adhesive decreased the minimum welding current required for obtaining a sufficiently sized nugget.

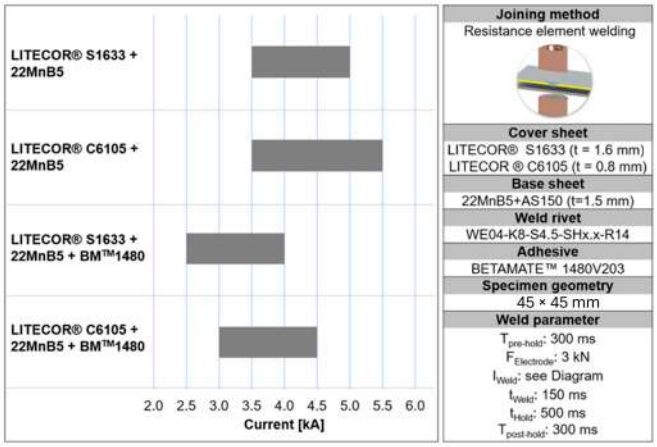

Figure 17. Comparison of the welding current ranges between I_{min} and I_{max} for two hybrid material configurations (0.8 mm/1.6 mm) welded with 22MnB5, with and without additional adhesive. Reprinted with permission from Ref. [96]. Copyright 2024 Springer Nature.

8. Strength and Failure Mode of REW Joints

The tensile-shear (TS) test can determine the mechanical performance of REW welds. Tensile shear is the most widely used test because sample preparation in this method is simple and appropriate for evaluating the mechanical properties of the REW joints. The peak load (load-bearing capacity) and energy absorption can be extracted from the load–displacement curve of the tensile shear test [66]. They are defined, respectively, as the maximum force achieved during the test and the energy absorbed by the specimen (i.e., the area under the force-displacement curve) from the beginning of the test up to the peak load. Table 1 shows the mechanical properties of REW joints based on studies by researchers.

Table 1. The mechanical properties of REW joints in the optimum condition based on the literature (* welding current, welding time, electrode force).

Author	Materials	Process	Parameters *	Peak Load (PL) and Energy Absorption (EA)
Manladan et al. [16]	AZ31 Mg/316 L ASS	REW	5–9 kA 250 ms 3.6 kN	PL = 3.71 kN EA = 10.19 J 8 kA
Manladan et al. [42]	AZ31 Mg/316 L ASS	REWB	5–9 kA 150 ms 3.6 kN	PL = 7.54 kN EA = 52 J 8 kA
Manladan et al. [81]	AZ31 Mg/316 L ASS/316 L ASS	REW	5–10 kA 180 ms 3.6 kN	PL = 9.3 kN EA = 83 J 10 kA
Troschitz et al. [97]	TPC composite/low-alloyed steel	REW	9–13 kA 40–70 ms 3 kN	PL = 3.7 kN 11 kA
Cai et al. [12]	DP780/AA5052	REW	12–22 kA 15 cycles 3 kN	PL = 5.7 kN 21 kA
Ling et al. [6]	22MnMoB steel/AA6061-T6	REW	6–10 kA 300 ms 3.6 kN	PL = 5.7 kN 18 kA
Ling et al. [5]	DP780/AA6061-T6	REW	6–10 kA 300 ms 3.6 kN	PL = 7.36 kN EA = 18.19 J 7 kA
Niu et al. [61]	AA6061/HS1300T steel	REW	5–9 kA 200 ms 2 kN	PL = 5.21 kN 7 kA
Sun et al. [26]	AA6061/DP600	MA-REW	8–11 kA 200 ms 3 kN	PL = 6.7 kN 11 kA
Duric et al. [43]	AA5754-H22/DP500	REW	6–10 kA 60 ms 3.68 kN	PL = 2.5 kN EA = 5.7 J 6 kA
Fei et al. [60]	AA6061/Q235 steel	Flat REW (FREW)	11–15 kA 300 ms 3.6 kN	PL = 5.6 kN EA = 16.55 J 14 kA

The failure mode of welded joints is an indicator of joint quality, serving as a qualitative measure of their energy absorption and load-bearing capabilities [16]. This evaluation is an important criterion for assessing the mechanical performance of RSW and REW welds. Figure 18 shows the different failure modes that can generally be observed in REW joints. During tensile shear testing, fractures typically initiate at points A and B, which correspond

to the weld edges of the joint. These locations experience the highest stress concentrations, making them prone to crack nucleation. Once initiated, these cracks propagate toward the rivet, leading to different failure modes. The two primary failure modes most commonly found in REW joints are interfacial (IF) and pullout fractures (PFs), as depicted in Figure 18. In the IF mode, joint strength is closely related to the characteristics of the weld nugget [61]. If the nugget lacks sufficient strength to withstand the tensile shear force, the crack readily propagates along the rivet/bottom sheet interface through the nugget [60]. In contrast, the PF mode is preferred in the automotive industry, as it indicates that the joint strength mainly relies on the upper alloy sheet, which is typically the weaker material [61]. In the PF mode, the nugget remains firmly attached to the rivet, making plastic deformation more difficult. Cracks nucleated under tensile stress propagate along the nugget edge with the lowest hardness until the nugget is eventually pulled out. Another failure mode, base-metal fracture, can occur when excessively high welding currents decrease the hardness of the upper sheet [12] or when there is a significant difference in hardness between the nugget and the upper sheet. Although achieving this failure mode in RSW is difficult (with IF being more common [98–100]), the predominant failure mode in REW joints is PF [6,16,43,97]. Studies by Manladan et al. [16] and Niu et al. [61] on REW joints of magnesium alloy/ASS and aluminum 6061 T-6 and stainless steel revealed that, at a welding current of 5 kA, the REW joints failed in the IF mode. However, as the welding current increased, the failure mode shifted to PF.

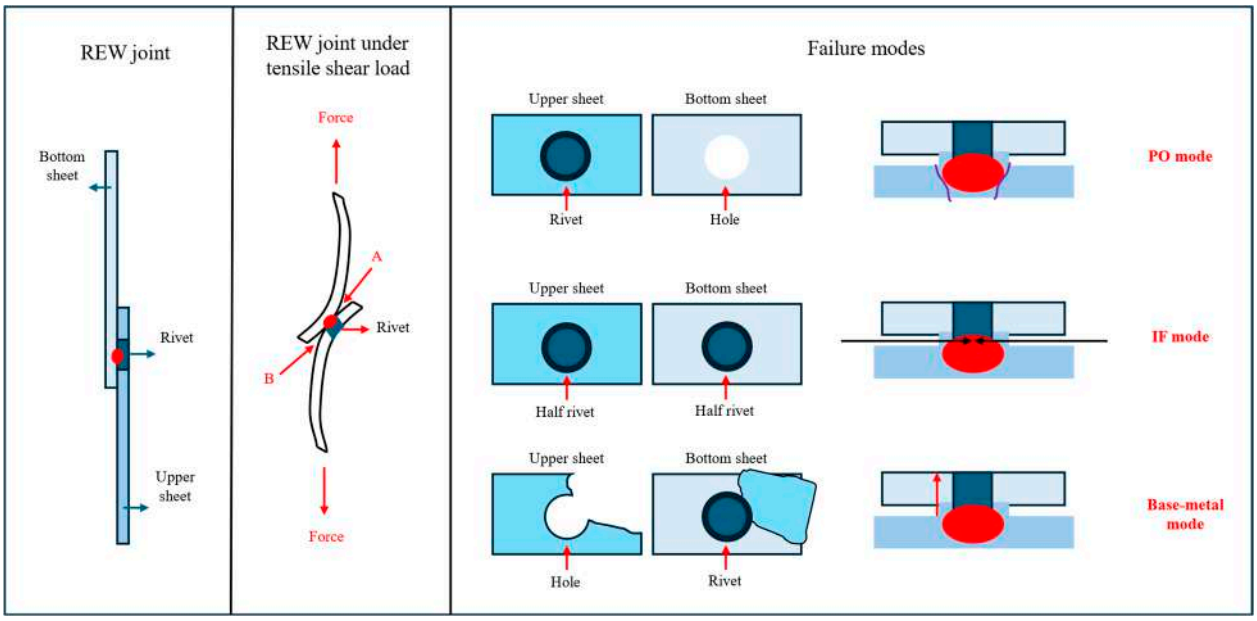

Figure 18. Failure modes in the REW joining process.

Figure 19 shows the tensile curves for the uncoated boron steel and aluminum 6061 REW joint, welded using three different currents: 16 kA for RSW and 7 and 9 kA for REW [6]. After reaching their peak loads, the curves for the 16 kA RSW and 7 kA REW dropped abruptly, indicating a brittle fracture with an IF failure. In contrast, the 9 kA REW curve showed a more gradual decrease, which is associated with a PF failure mode. SEM analysis revealed that, while the 7 kA REW sample had numerous dimples on its fracture surface, their small size limited the energy absorption capability. On the other hand, the 9 kA REW joint showed the rivet securely welded to the steel, causing failure in the weaker base material. This failure mode was identified by Ling et al. [6] as the base-metal fracture mode. The fracture surface of this joint displayed numerous large dimples, making it more resistant and capable of absorbing energy. The joints exhibiting the IF failure mode (16 kA RSW and 7 kA REW) demonstrated load–displacement behavior similar to Figure 19a,b, while the base-metal fracture mode (9 kA REW) had a behavior like Figure 19c.

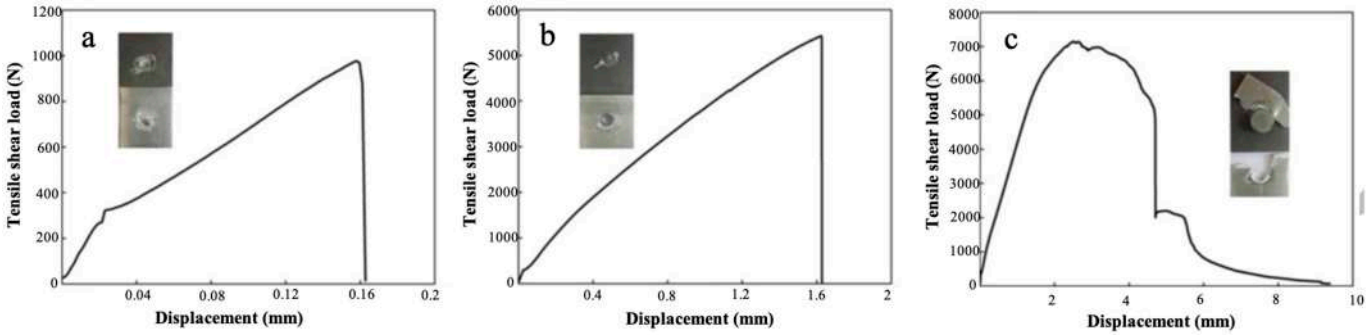

Figure 19. Tensile curves of (**a**) 16 kA RSW joint, (**b**) 7 kA REW joint, and (**c**) 9 kA REW joint. Reprinted with permission from Ref. [6]. Copyright 2024 Taylor & Francis.

Duric et al. [43] investigated REW joints between DP500 steel and an aluminum alloy. Three different welding currents were tested: 6 (REW-1), 8, (REW-2), and 10 kA (REW-3). The load–displacement curves in Figure 20 indicate that increasing the welding current did not significantly improve mechanical strength. Figure 20b shows that all the specimens failed in the PF mode. They also observed secondary bending in the aluminum sheet, which led to a compressed region on the primary bearing surface under the rivet. As the tensile test progressed, this compressed region enlarged, finally causing sudden failure through the hole center. This type of failure was attributed to the limited ductility and reduced stiffness of the aluminum alloy.

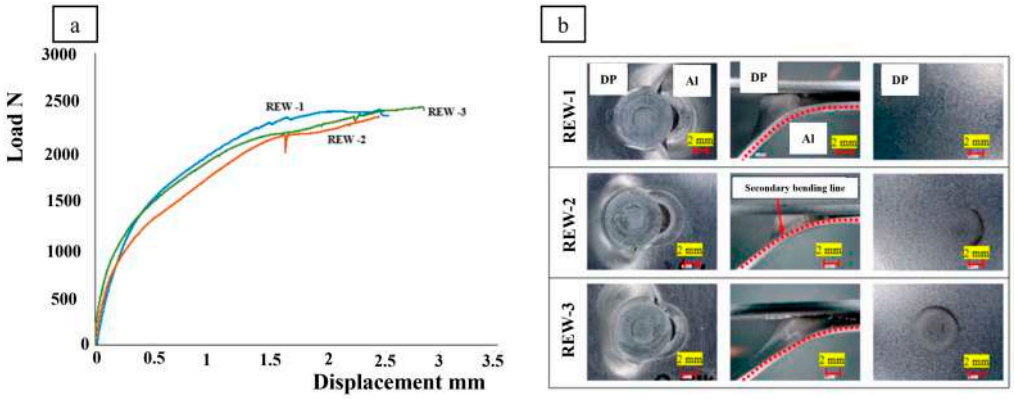

Figure 20. (**a**) Tensile-shear load–displacement curves of Al/steel REW joints and (**b**) their fracture surface morphologies. Reprinted from Ref. [43].

As previously discussed, excessive heat input can be detrimental to mechanical properties, such as energy absorption and strength. Initially, peak load and energy absorption increase with the welding current, but beyond a certain point, these properties begin to reduce [16,59]. Manladan et al. [16] identified a threshold in the welding current–load curve for joints between magnesium alloy and 316 L stainless steel, attributed to excessive heat causing localized melting of magnesium around the rivet, which widened the rivet hole. Similarly, in RSW joints, a decrease in peak load was observed due to metal expulsion [42]. Expulsion-induced shrinkage and hole formation compromised weld quality [42]. Wang et al. [79] found that expulsion occurred in REW joints between aluminum and titanium when welding currents increased to 8 and 10 kA for 6 and 8 mm diameter rivets, respectively. Figure 21a demonstrates that, at the same welding current, an 8 mm diameter rivet joint produced a larger nugget diameter than a 6 mm diameter rivet joint. Nugget size further increased with welding current. However, as depicted in Figure 21b, beyond a certain limit, increasing nugget size did not enhance mechanical properties. While load and energy absorption initially peaked at 8 and 10 kA for 6 and 8 mm diameter rivet joints, further current increases reduced mechanical resistance due to metal expulsion.

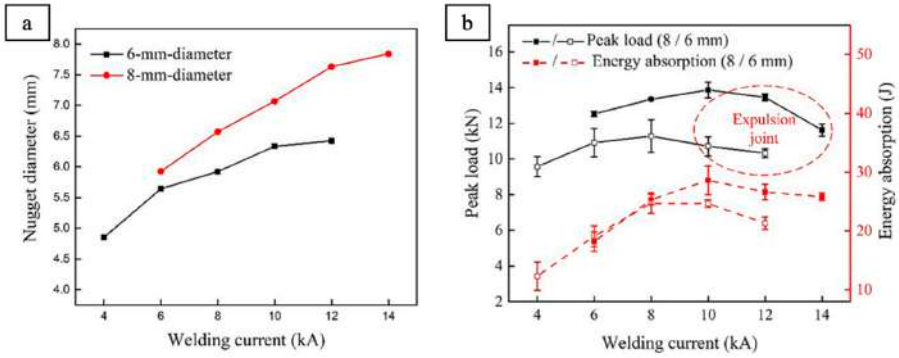

Figure 21. Nugget diameters and lap-shear properties of REW joints: (**a**) nugget diameter; (**b**) peak load and energy absorption. Reprinted with permission from Ref. [79]. Copyright 2024 Elsevier.

Manladan et al. [16] also examined REWB joints between ASS and magnesium alloy. Figure 22 shows the load–displacement curves for different joining methods: AB, RSW, REW, RSWB, and REWB. Figure 22a shows that AB joints experienced three stages: initially, a rapid load increase, a gradual increase, and a sharp drop in the final stage. This failure mode was deemed unsuitable for automotive applications due to its poor crashworthiness. During tensile shear testing, the joining area may experience rotation due to plastic deformation [42], a phenomenon known as secondary bending or out-of-plane displacement. REW joints displayed a PO failure mode, as shown in Figure 22a. Their load–displacement curve is similar to that of AB joints in the first two stages; however, the load decreased more gradually as the nugget pulled out in the third stage. REW joints also experienced greater out-of-plane deformation than AB joints. Despite larger ductility, AB joints exhibited higher strength. As a result, REWB joints displayed hybrid behavior combining characteristics of both AB and REW joints. Their load–displacement curve, as shown in Figure 22b, consisted of five stages: a rapid load increase (comparable to the AB joint), a slower increase to the peak load (larger than the peak loads of AB and REW), a sharp drop due to adhesive failure, followed by a secondary load increase (the REW component continued bearing the load), and final PO failure. Figure 22b,c indicates that, while AB, RSW, and RSWB joints experienced IF failure modes, REWB joints exhibited superior mechanical performance compared to RSWB joints.

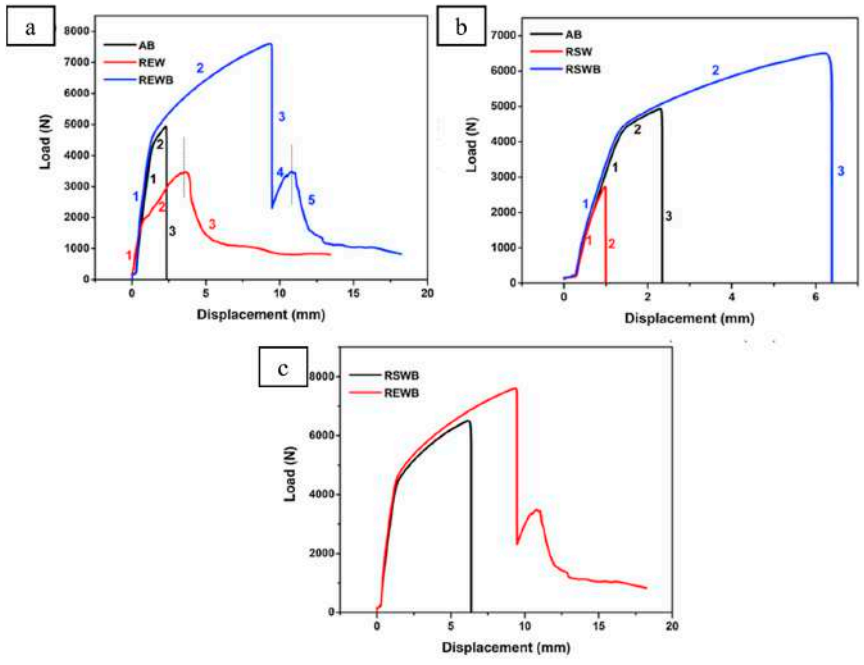

Figure 22. (**a**–**c**) Typical L–D Curves of REW, AB, RSWB, RSW, and REWB joints. Reprinted with permission from Ref. [42]. Copyright 2024 Elsevier.

9. Fatigue of REW Joints

A notch at the faying interface of a weld acts as a stress concentration site or as a pre-existing crack, making the joint susceptible to fatigue failure under dynamic loading conditions. Fatigue accounts for over 90% of operational component failures [101–103], pointing out its critical role in the durability of weld-bonded joints [104,105]. Several studies [69,106,107] have demonstrated that factors such as the type of loading, sheet thickness, and nugget diameter significantly affect the fatigue behavior of aluminum RSW joints. Florea et al. [69] investigated the fatigue behavior of the aluminum 6061 RSW joints, categorizing the samples based on welding current and electrode force into low, nominal, and high levels, corresponding to low, medium, and high welding currents, respectively. Their findings indicated that the failure mode varied with changes in welding current. Hassanifard et al. [106] assessed the role of electrode force in the mechanical behavior of aluminum 5083 spot-welded joints. They found that increasing the electrode force from 2500 to 3000 N had little effect on nugget size and fatigue strength. However, further increasing the electrode force to 3500 N, despite a slight reduction in nugget diameter, significantly improved the joint's fatigue life.

Ling et al. [5] studied the fatigue behavior of RSW/REW joints between DP780 steel and aluminum 6061-T6. They estimated the fatigue limit of REW and RSW joints to be 1800 and 900 N, respectively. At high-cycle fatigue (HCF), both types of joints exhibited through-thickness fractures (Figure 23b,d). However, under low-cycle fatigue (LCF), RSW joints failed in PO mode (Figure 23a), while REW joints exhibited IF fractures (Figure 23c). Fractographic analysis revealed that in the through-thickness fracture mode, cracks initiated at the center and edges of the aluminum sheet, then propagated through its thickness and width. This resulted in a brittle fracture surface with numerous dimples, indicating rapid crack propagation in the final stage. In the IF fracture mode, an "eyebrow" crack formed at the initiation site, with the development of elongated dimples, and the crack propagated quickly along the faying surface, where cleavage planes were present. In the PO failure mode, cracks initiated at the surface of the steel sheet and propagated through its thickness, generating a complex fracture surface with a mixture of dimples and cleavage planes.

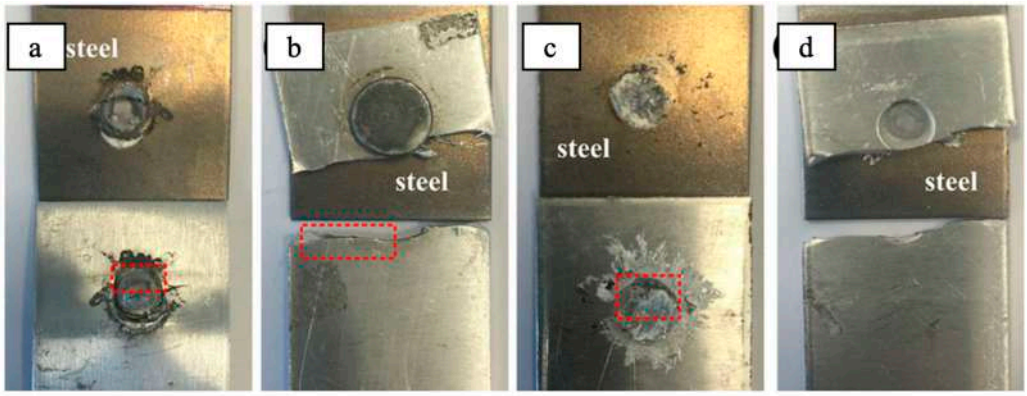

Figure 23. Fatigue fracture appearances of the REW joints fractured at (**a**) 5500 N and 18,000 cycles and (**b**) 3000 N and 330,000 cycles, and the RSW joints fractured at (**c**) 2500 N and 98,000 cycles and (**d**) 1400 N and 1,800,000 cycles. Reprinted with permission from Ref. [5]. Copyright 2024 Springer Nature.

Duric et al. [43] investigated the fatigue behavior of REW joints between aluminum alloy and DP500 steel. The S-N curve for the REW joint, as shown in Figure 24, indicates a fatigue limit of 882 N at 10^7 cycles. In all tested specimens, fractures consistently occurred within the aluminum section of the joint. The crack initiation site was primarily located under the rivet on the aluminum surface, attributed to the lower hardness of the aluminum alloy compared to the steel. In addition, the presence of an IMC layer near the weld was identified as a factor contributing to crack initiation and propagation at this location. Rao

et al. [108] investigated the fatigue properties of dissimilar Al6022/IF steel RSW joints, reporting a similar fatigue strength of 920 N at 10^7 cycles. Uematsu et al. [109] found a fatigue strength of 20 MPa at 10^7 cycles for dissimilar FSSW joints of Al6061/steel. Okane et al. [110] studied the fatigue behavior of FSW Al/steel joints and reported a value of 40 MPa at 10^7 cycles.

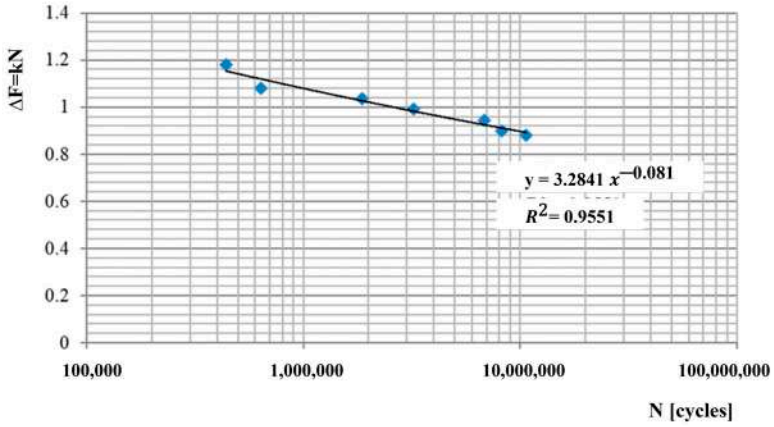

Figure 24. Fatigue S–N curve of REW joints between aluminum alloy and DP500 steel (welding current 10 kA). Reprinted from Ref. [43].

10. Numerical Studies and Simulation

As discussed earlier, the failure mode of a weld joint is influenced by the nugget size and the mechanical properties of the lighter sheet. Nugget size is a crucial factor in determining joint quality, with a larger nugget size generally improving the joint's mechanical properties [94]. In RSW, a commonly used equation for estimating the minimum nugget size with adequate mechanical strength is $D = 4\ t^{0.5}$, where D is the nugget diameter and t is the sheet thickness. However, this conventional equation only considers the sheet thickness, which can lead to inaccuracies in some cases [82]. Pouranvari et al. [111] developed an analytical model to estimate the minimum nugget size and predict the failure mode transition for RSW of AHSSs. Their model is expressed as $Dc = 8t\ (H_{PFL}/H_{WN})$ where H_{PFL} and H_{WN} are the hardness values at the pull-off location and the nugget, respectively, and t is the thickness of the sheet stack. Nevertheless, this model, designed for RSW joints, cannot be directly applied to REW joints, which are hybrid mechanical-metallurgical welds. In addition, these equations only hold for similar material combinations [61]. To address this limitation, Fei et al. [94] modified Pouranvari's [111] model for FREWB joints between Q235 steel and aluminum 6061 alloy, introducing a welding intention factor:

$$D_C = 8\ m\ t\ (H_{PFL}/H_{WN}) \quad (3)$$

where m is the indentation rate of the steel plate. According to Pouranvari et al. [111], PF fracture typically initiates at the point of lowest hardness through localized necking in the thickness direction, whereas IF fracture results from shear stresses acting on the nugget. Therefore, tensile and yield strength estimates can be derived from the average hardness of the lowest hardness zone [112]. Other models are available for calculating peak loads, including those proposed by the Architectural Institute of Japan (AIJ), AISC-LRFD, Eurocode 3 (EN 1993-1-8:2005 [113]), and the block shear model in CAN/CSA-S16-09 [61]. To identify the most accurate model, a test-to-predicted ratio is calculated and validated against actual peak load values [61]. Niu et al. [61] applied the AIJ model to determine the minimum nugget size in REW joints, assuming the θ angle as zero, a uniform shear stress distribution at the weld interface, and a cylindrical nugget with diameter d:

$$d = 0.99\sqrt{P/HV_{FZ}} \quad (4)$$

where d is the nugget diameter, and P is defined as one-third of the FZ hardness (HV_{FZ}). According to this model, if the nugget size exceeds the critical value, the joint will fail in the PF mode; otherwise, it will fail in the IF mode. Niu et al. [61] discovered that the critical nugget size for integrated REW joints of aluminum 6061 and stainless steel is approximately 3.24 mm.

Rao et al. [114] used numerical simulation to investigate nugget shifting and its prevention in the REW joining of Q235 and DP steel. Their study considered multiple interfacial contacts, as well as the electrical, thermal, and mechanical characteristics of the welding process. Using a 3D fully coupled method in Abaqus, they simulated both RSW and REW processes. The results indicated that REW effectively reduced nugget shifting between plates and minimized heat transfer to the electrode compared to RSW. The nugget formed at a lower welding current and with a shorter welding time in REW. This technique also lowered the electrode temperature, extending its lifespan. In addition, the introduction of an insulation layer in REW further enabled the formation of larger nugget sizes at reduced current levels.

11. REW Joining of Hybrid Materials/Composites with Steel

Hybrid materials such as ALUCOBOND®, HYLITE®, GLARE®, LITECOR™, and BONDAL® have attracted significant interest in multi-material structures featuring polymer-based cores and metallic cover layers. These materials offer a combination of high damping, bending stiffness, and low density, making them promising alternatives to traditional lightweight metals like aluminum alloys [96]. However, their composition poses some challenges for thermal joining processes, making the REW technique a preferred solution. Holtschke and Jüttner [37] studied the REW and adhesive bonding of LITECOR™ (metallic cover layers and polymer-based cores) with press-hardened 22MnB5 steel. They used capacitor discharge (CD) welding to join these materials with extremely short welding times (5–40 ms) and rapid current increases. This method aimed to minimize thermal damage to the LITECOR™ polymer core by reducing the welding duration, thereby avoiding undesirable effects such as blistering and delamination, as shown in Figure 25. Inspections of the joint cross-sections confirmed that the sandwich material remained undamaged despite the higher energy input and associated displacement. Additionally, no weld nugget was observed at the joining interface due to the very short welding time.

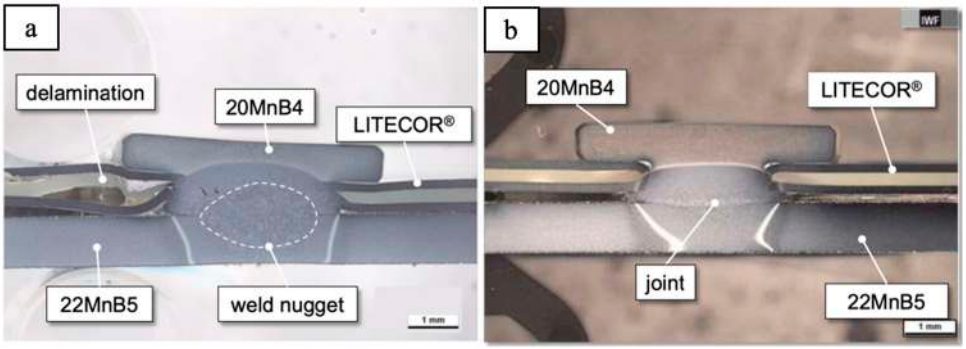

Figure 25. Macro images of (**a**) conventional MF-DC equipment and (**b**) CD welding. Reprinted with permission from Ref. [37]. Copyright 2024 Springer Nature.

Schmal and Meschut [96] investigated the influence of production-related disturbance variables (factors or variations that affect the consistency, stability, and quality of the joint being formed) and polarity influences on REW joints between LITECOR™ of two different thicknesses of 0.8 and 1.6 mm and steel. They examined the effects of electrode-cap offset, varying it from a 0 to 3 mm range in 0.5 mm increments. For joints with thinner LITECOR™, an increase in electrode offset resulted in a larger nugget diameter. In contrast, the nugget size remained almost unchanged despite increased welding current in joints with thicker LITECOR™. This difference was attributed to the greater rivet

stability and guidance in thicker sheets, while in thinner sheets, rivet tilting led to higher resistance and heat input, causing the formation of larger nuggets. However, excessive heat can be detrimental to hybrid materials with polymer-based cores, as they are sensitive to thermal damage. The study also revealed that gaps of up to 1.5 mm at the faying interface did not significantly affect nugget diameter, but such gaps could increase corrosion risks in industrial applications. The use of adhesives proved effective in achieving high-quality joints with lower welding currents. Interestingly, changes in polarity did not influence nugget size in REW joints. Troschitz et al. [97] studied the joining of thermoplastic composites (TPC) and steel sheets without damaging the fibers. They assessed joint quality using single-lap shear and chisel tests with different rivet designs. Welding process simulations helped determine optimal welding parameters. Among the rivets tested, the design with a larger undercut volume demonstrated superior performance, achieving a higher ultimate pull-out load of around 3.7 kN.

12. Benefits and Limitations of REW

REW is a highly efficient and innovative joining process that offers several benefits, particularly in the automotive and aerospace industries, where lightweight and high-strength components are increasingly used. The advantage of REW lies in its ability to join dissimilar materials with notably different physical and chemical properties, such as aluminum and steel, which are challenging for most conventional fusion welding techniques. REW is inherently efficient, as it generates heat by electrical resistance, which is localized at the contact points between materials. This minimizes thermal distortion and preserves the properties of the base materials. Integrating a mechanical element, such as a stud or pin, enhances joint strength and reliability, making REW especially suitable for structural applications. In addition, the process produces minimal waste and does not require additional filler materials or shielding gases, making it cost-effective and environmentally friendly. The process is also highly repeatable, making it suitable for automation in high-volume manufacturing environments, allowing for high-speed production and consistent weld quality. In this regard, existing resistance spot welding equipment can often be adapted for REW, requiring only an additional machinery investment in a riveting machine to insert the joining element in the upper part.

Despite its many advantages, REW has some limitations that may constrain its adoption. Designed primarily for lap joints, REW is unsuitable for other joint configurations, which restricts design flexibility. Its reliance on resistance heating necessitates careful management of material thickness and electrical conductivity to achieve optimal results, potentially limiting its use for certain material combinations or very thick sections. Surface preparation is another critical factor, as contaminants such as oil or pre-existing superficial oxides can significantly degrade weld quality. The use of a third element (rivet or stud) adds weight and complexity to the process. While some joining elements can self-punch through materials, pre-drilling may be required for stronger upper components, introducing an additional step not required in traditional resistance spot welding. This can lead to stress concentrations that may remain in the joints after welding. The join element also requires precise positioning, as it needs to be centered within the parts to avoid misalignment and ensure strength. Consequently, the process is sensitive to robot tolerances and requires access to the weld area from both sides for electrode placement, which may limit its applicability in confined spaces. Moreover, joining dissimilar metals also raises the risk of galvanic corrosion, necessitating coatings or pre-treatment of the elements. While REW is robust and adaptable in many contexts, its adoption may be hindered by the need for skilled operators and rigorous quality control measures to ensure reliable and repeatable joints. Finally, the absence of established industry standards and the presence of competing technologies, such as FEW and Flow Drilling Screw (FDS), which may offer superior mechanical performance or lower costs in specific applications, pose challenges to the wider adoption of REW.

Despite these challenges, REW remains a valuable technique for applications demanding strong, lightweight, and high-performance joints. Its unique combination of adaptability, precision, and compatibility with advanced materials ensures its relevance in industries where innovation and structural integrity are paramount.

13. Future Trends

To date, most research on REW has primarily focused on joining steel with aluminum and magnesium alloys, particularly the 5xxx and 6xxx aluminum grades and AZ31 magnesium alloys. However, many other material combinations hold potential for developing lightweight and resistant assembled components. For instance, the 7xxx series aluminum alloys, despite their limited weldability, are widely used in the automotive industry but remain under-investigated in the context of REW [115,116]. Similarly, titanium/steel joints in REW offer promising solutions for applications requiring high specific strength, whereas copper/steel joints are ideal for scenarios that demand excellent thermal and electrical conductivity alongside high strength. Furthermore, exploring dissimilar joining of non-ferrous materials, including metallic and non-metallic combinations, could open new frontiers across various industries.

A significant factor affecting the sustainability and cost-effectiveness of REW is electrode degradation. Enhancing electrode durability is therefore critical to extending the lifespan and improving the economic viability of REW applications [117–120]. Innovations, such as experimenting with rivets of different shapes or employing headless rivets, could improve joint strength and contribute to weight reduction in components.

Residual stresses also play a crucial role in determining the performance of REW joints, affecting properties such as strength, joint integrity, and durability [121,122]. These stresses are mainly caused by material volumetric contraction during solidification and expansion during heating cycles, with tensile residual stresses being particularly detrimental to strength, fatigue performance, and dimensional stability. Advanced characterization techniques, such as neutron scattering diffraction and X-ray diffraction, could be used to investigate the influence of these stresses on REW joint performance.

Fatigue strength is another critical consideration, particularly for automotive components where welded joints are often subject to stress concentrations [102]. One common stress concentration point is the gap between two sheets at successive REW joints. In addition, intermetallic compounds formed between the rivet and the upper sheet serve as primary sites for crack initiation [43]. While research has been conducted on the fatigue strength of dual-phase (DP) steel and aluminum alloy joints, there remains a significant gap in understanding the fatigue behavior of REW joints involving steel and non-ferrous alloys such as magnesium or titanium alloys. Similarly, fatigue studies on REW joints comprising entirely non-ferrous alloys, such as aluminum/magnesium, titanium/magnesium, or titanium/aluminum, remain unexplored. Investigating key variables, including loading type, sheet thickness, and nugget diameter, is recommended for addressing these knowledge gaps.

Given the extensive use of REW joints in automotive assemblies, understanding their fatigue behavior is crucial to ensuring vehicle crashworthiness and long-term reliability. Future research should address these gaps to optimize REW processes and meet the evolving demands of the automotive industry.

14. Summary

In recent years, stricter regulations aimed at reducing greenhouse gas emissions have placed significant pressure on the automotive industry, a major contributor to these emissions. One effective strategy to lower emissions is reducing vehicle weight, which has driven interest in replacing steel with lightweight materials such as composites and hybrid materials in multi-material structures. Therefore, efficient joining techniques for these dissimilar materials have become crucial. RSW is a fast, cost-effective, and widely used joining method, but it faces challenges when applied to dissimilar materials. The

recent REW technique, an advancement of RSW, offers a promising alternative. This article has presented a comprehensive review of REW's potential for joining different dissimilar materials. It also compared the mechanical properties of welded joints, highlighting the advantages and limitations of REW in comparison to other joining methods. In addition, the article has discussed the critical role of nugget size on joint strength, fatigue behavior, modeling, corrosion resistance, and microstructure. Despite significant progress, several research gaps remain in REW technology. The authors hope this article contributes to advancing the understanding and development of dissimilar material joining methods and emphasizes the need for further research in this field.

Author Contributions: Conceptualization, M.A., M.D.M., V.R. and P.R.S.; formal analysis, M.A., M.D.M., V.R. and P.R.S.; investigation, M.A. and P.R.S.; data curation, M.A.; writing—original draft preparation, M.A. and P.R.S.; writing—review and editing, M.A., M.D.M., V.R. and P.R.S.; supervision, P.R.S. All authors have read and agreed to the published version of the manuscript.

Funding: This research received no external funding.

Data Availability Statement: No new data were created or analyzed in this study.

Conflicts of Interest: The authors declare no conflicts of interest.

References

1. Frondel, M.; Schmidt, C.M.; Vance, C. A regression on climate policy: The European Commission's legislation to reduce CO_2 emissions from automobiles. *Transp. Res. Part A Policy Pract.* **2011**, *45*, 1043–1051. [CrossRef]
2. Jannesar Niri, A.; Poelzer, G.A.; Zhang, S.E.; Rosenkranz, J.; Pettersson, M.; Ghorbani, Y. Sustainability challenges throughout the electric vehicle battery value chain. *Renew. Sustain. Energy Rev.* **2024**, *191*, 114176. [CrossRef]
3. Manladan, S.M.; Yusof, F.; Ramesh, S.; Fadzil, M. A review on resistance spot welding of magnesium alloys. *Int. J. Adv. Manuf. Technol.* **2016**, *86*, 1805–1825. [CrossRef]
4. Witik, R.A.; Payet, J.; Michaud, V.; Ludwig, C.; Månson, J.A.E. Assessing the life cycle costs and environmental performance of lightweight materials in automobile applications. *Compos. Part A Appl. Sci. Manuf.* **2011**, *42*, 1694–1709. [CrossRef]
5. Ling, Z.; Li, Y.; Luo, Z.; Ao, S.; Yin, Z.; Gu, Y.; Chen, Q. Microstructure and fatigue behavior of resistance element welded dissimilar joints of DP780 dual-phase steel to 6061-T6 aluminum alloy. *Int. J. Adv. Manuf. Technol.* **2017**, *92*, 1923–1931. [CrossRef]
6. Ling, Z.; Li, Y.; Luo, Z.; Feng, Y.; Wang, Z. Resistance Element Welding of 6061 Aluminum Alloy to Uncoated 22MnMoB Boron Steel. *Mater. Manuf. Process.* **2016**, *31*, 2174–2180. [CrossRef]
7. Badkoobeh, F.; Mostaan, H.; Rafiei, M.; Bakhsheshi-Rad, H.R.; Berto, F. Microstructural Characteristics and Strengthening Mechanisms of Ferritic–Martensitic Dual-Phase Steels: A Review. *Metals* **2022**, *12*, 101. [CrossRef]
8. Rana, R.; Lahaye, C.; Ray, R.K. Overview of Lightweight Ferrous Materials: Strategies and Promises. *JOM* **2014**, *66*, 1734–1746. [CrossRef]
9. Hirsch, J.; Al-Samman, T. Superior light metals by texture engineering: Optimized aluminum and magnesium alloys for automotive applications. *Acta Mater.* **2013**, *61*, 818–843. [CrossRef]
10. Galán, J.; Samek, L.; Verleysen, P.; Verbeken, K.; Houbaert, Y. Advanced high strength steels for automotive industry. *Rev. Metal.* **2012**, *48*, 118–131. [CrossRef]
11. Martinsen, K.; Hu, S.J.; Carlson, B.E. Joining of dissimilar materials. *CIRP Ann.* **2015**, *64*, 679–699. [CrossRef]
12. Cai, W.; Chen, Q.; Wang, Y.; Dong, S.; Luo, P. Microstructural and mechanical characterization of steel-DP780/Al-5052 joints formed using resistance element welding with concealed rivet cover. *Compos. Adv. Mater.* **2022**, *31*, 263498332211010. [CrossRef]
13. Qiu, R.; Iwamoto, C.; Satonaka, S. Interfacial microstructure and strength of steel/aluminum alloy joints welded by resistance spot welding with cover plate. *J. Mater. Process. Technol.* **2009**, *209*, 4186–4193. [CrossRef]
14. Hayat, F. Resistance Spot Weldability of Dissimilar Materials: BH180-AISI304L Steels and BH180-IF7123 Steels. *J. Mater. Sci. Technol.* **2011**, *27*, 1047–1058. [CrossRef]
15. Pouranvari, M.; Marashi, S.P.H. Critical review of automotive steels spot welding: Process, structure and properties. *Sci. Technol. Weld. Join.* **2013**, *18*, 361–403. [CrossRef]
16. Manladan, S.M.; Yusof, F.; Ramesh, S.; Zhang, Y.; Luo, Z.; Ling, Z. Resistance Element Welding of Magnesium Alloy/austenitic Stainless Steel. *IOP Conf. Ser. Mater. Sci. Eng.* **2017**, *238*, 012004. [CrossRef]
17. Bader, B.; Türck, E.; Vietor, T. Multi material design. A current overview of the used potential in automotive industries. In *Technologies for Economical and Functional Lightweight Design*; Springer: Berlin/Heidelberg, Germany, 2019; pp. 3–13. [CrossRef]
18. Zhang, T.; Wang, W.; Liu, J.; Wang, L.; Tang, Y.; Wang, K. A review on magnesium alloys for biomedical applications. *Front. Bioeng. Biotechnol.* **2022**, *10*, 953344. [CrossRef] [PubMed]
19. Yang, Y.; Xiong, X.; Chen, J.; Peng, X.; Chen, D.; Pan, F. Research advances of magnesium and magnesium alloys worldwide in 2022. *J. Magnes. Alloys* **2023**, *11*, 2611–2654. [CrossRef]

20. Liu, B.; Yang, J.; Zhang, X.; Yang, Q.; Zhang, J.; Li, X. Development and application of magnesium alloy parts for automotive OEMs: A review. *J. Magnes. Alloys* **2023**, *11*, 15–47. [CrossRef]
21. Yang, Y.; Xiong, X.; Chen, J.; Peng, X.; Chen, D.; Pan, F. Research advances in magnesium and magnesium alloys worldwide in 2020. *J. Magnes. Alloys* **2021**, *9*, 705–747. [CrossRef]
22. Yang, J.; Song, Y.; Dong, K.; Han, E.H. Research progress on the corrosion behavior of titanium alloys. *Corros. Rev.* **2023**, *41*, 5–20. [CrossRef]
23. Li, G.; Chandra, S.; Rahman Rashid, R.A.; Palanisamy, S.; Ding, S. Machinability of additively manufactured titanium alloys: A comprehensive review. *J. Manuf. Process.* **2022**, *75*, 72–99. [CrossRef]
24. Zhao, Q.; Sun, Q.; Xin, S.; Chen, Y.; Wu, C.; Wang, H.; Xu, J.; Wan, M.; Zeng, W.; Zhao, Y. High-strength titanium alloys for aerospace engineering applications: A review on melting-forging process. *Mater. Sci. Eng. A* **2022**, *845*, 143260. [CrossRef]
25. Zhang, T.; Liu, C.T. Design of titanium alloys by additive manufacturing: A critical review. *Adv. Powder Mater.* **2022**, *1*, 100014. [CrossRef]
26. Sun, Y.; Huang, R.; Zhao, H.; Chen, X.; Jiang, M.; Wu, L.; Chen, B.; Tan, C. Enhancement of resistance element welding of AA6061 to DP600 steel by using external magnetic field. *J. Manuf. Process.* **2022**, *80*, 347–358. [CrossRef]
27. Kalyankar, V.; Chudasama, G. On the metallurgical challenges of intermetallic compound in steel/Al dissimilar resistance spot welding: Significance, growth and controlling mechanisms. *Adv. Mater. Process. Technol.* **2024**, *10*, 2062–2094. [CrossRef]
28. Stavropoulos, P.; Sabatakakis, K. Quality Assurance in Resistance Spot Welding: State of Practice, State of the Art, and Prospects. *Metals* **2024**, *14*, 185. [CrossRef]
29. Xu, T.; Shi, Y.; Cui, Y.; Liang, Z. Effects of Magnetic Fields in Arc Welding, Laser Welding, and Resistance Spot Welding: A Review. *Adv. Eng. Mater.* **2023**, *25*, 2200682. [CrossRef]
30. Martín, Ó.; De Tiedra, P. Advances in the Control and Improvement of Quality in the Resistance Spot Welding Process. *Metals* **2022**, *12*, 1810. [CrossRef]
31. Soomro, I.A.; Pedapati, S.R.; Awang, M. A review of advances in resistance spot welding of automotive sheet steels: Emerging methods to improve joint mechanical performance. *Int. J. Adv. Manuf. Technol.* **2021**, *118*, 1335–1366. [CrossRef]
32. Shah, L.H.; Ishak, M. Review of Research Progress on Aluminum–Steel Dissimilar Welding. *Mater. Manuf. Process.* **2014**, *29*, 928–933. [CrossRef]
33. Lan, S.; Liu, X.; Ni, J. Microstructural evolution during friction stir welding of dissimilar aluminum alloy to advanced high-strength steel. *Int. J. Adv. Manuf. Technol.* **2016**, *82*, 2183–2193. [CrossRef]
34. Shen, Z.; Yang, X.; Zhang, Z.; Cui, L.; Li, T. Microstructure and failure mechanisms of refill friction stir spot welded 7075-T6 aluminum alloy joints. *Mater. Des.* **2013**, *44*, 476–486. [CrossRef]
35. Cao, R.; Huang, Q.; Chen, J.H.; Wang, P.C. Cold metal transfer spot plug welding of AA6061-T6-to-galvanized steel for automotive applications. *J. Alloys Compd.* **2014**, *585*, 622–632. [CrossRef]
36. Abe, Y.; Kato, T.; Mori, K. Self-piercing riveting of high tensile strength steel and aluminium alloy sheets using conventional rivet and die. *J. Mater. Process. Technol.* **2009**, *209*, 3914–3922. [CrossRef]
37. Holtschke, N.; Jüttner, S. Joining lightweight components by short-time resistance spot welding. *Weld. World* **2016**, *2*, 413–421. [CrossRef]
38. He, X.; Zhao, L.; Yang, H.; Xing, B.; Wang, Y.; Deng, C.; Gu, F.; Ball, A. Investigations of strength and energy absorption of clinched joints. *Comput. Mater. Sci.* **2014**, *94*, 58–65. [CrossRef]
39. Mucha, J.; Kaščák, L.; Spišák, E. The Experimental Analysis of Forming and Strength of Clinch Riveting Sheet Metal Joint Made of Different Materials. *Adv. Mech. Eng.* **2013**, *5*, 11. [CrossRef]
40. Mucha, J. The analysis of lock forming mechanism in the clinching joint. *Mater. Des.* **2011**, *32*, 4943–4954. [CrossRef]
41. Mirza, F.A.; Macwan, A.; Bhole, S.D.; Chen, D.L.; Chen, X.G. Effect of welding energy on microstructure and strength of ultrasonic spot welded dissimilar joints of aluminum to steel sheets. *Mater. Sci. Eng. A* **2016**, *668*, 73–85. [CrossRef]
42. Manladan, S.M.; Zhang, Y.; Ramesh, S.; Cai, Y.; Luo, Z.; Ao, S.; Arslan, A. Resistance element weld-bonding and resistance spot weld-bonding of Mg alloy/austenitic stainless steel. *J. Manuf. Process.* **2019**, *48*, 12–30. [CrossRef]
43. Đurić, A.; Milčić, D.; Burzić, Z.; Klobčar, D.; Milčić, M.; Marković, B.; Krstić, V. Microstructure and Fatigue Properties of Resistance Element Welded Joints of DP500 Steel and AW 5754 H22 Aluminum Alloy. *Crystals* **2022**, *12*, 258. [CrossRef]
44. Sun, Y.F.; Fujii, H.; Takaki, N.; Okitsu, Y. Microstructure and mechanical properties of dissimilar Al alloy/steel joints prepared by a flat spot friction stir welding technique. *Mater. Des.* **2013**, *47*, 350–357. [CrossRef]
45. Chen, K.; Liu, X.; Ni, J. Effects of Process Parameters on Friction Stir Spot Welding of Aluminum Alloy to Advanced High-Strength Steel. *J. Manuf. Sci. Eng.* **2017**, *139*, 081016. [CrossRef]
46. Figner, G.; Vallant, R.; Weinberger, T.; Schröttner, H.; Pašič, H.; Enzinger, N. Friction Stir Spot Welds between aluminium and steel automotive sheets: Influence of welding parameters on mechanical properties and microstructure. *Weld. World* **2009**, *53*, R13–R23. [CrossRef]
47. Bozzi, S.; Helbert-Etter, A.L.; Baudin, T.; Criqui, B.; Kerbiguet, J.G. Intermetallic compounds in Al 6016/IF-steel friction stir spot welds. *Mater. Sci. Eng. A* **2010**, *527*, 4505–4509. [CrossRef]
48. Zhang, Y.; Xu, C.Y.; Peng, R.T.; Lei, B.; Jiang, J. A comparative study of self pierceing riveting and mechanical clinch of DP590-Al5754 high-strength steel and aluminum alloys. *Eng. Fail. Anal.* **2024**, *166*, 108835. [CrossRef]

49. Wang, C.; Du, Z.; Cheng, A.; He, Z. A comparative study on self-piercing riveting and pre-holed self-piercing riveting of high-strength steel and aluminum alloy. *Proc. Inst. Mech. Eng. Part L J. Mater. Des. Appl.* **2024**, 14644207241286111.
50. Jiang, H.; Gao, S.; Li, G.; Cui, J. Structural design of half hollow rivet for electromagnetic self-piercing riveting process of dissimilar materials. *Mater. Des.* **2019**, *183*, 108141. [CrossRef]
51. Lou, M.; Li, Y.; Wang, Y.; Wang, B.; Lai, X. Influence of resistance heating on self-piercing riveted dissimilar joints of AA6061-T6 and galvanized DP590. *J. Mater. Process. Technol.* **2014**, *214*, 2119–2126. [CrossRef]
52. Karathanasopoulos, N.; Mohr, D. Strength and Failure of Self-Piercing Riveted Aluminum and Steel Sheet Joints: Multi-axial Experiments and Modeling. *J. Adv. Join. Process.* **2022**, *5*, 100107. [CrossRef]
53. Oikawa, H.; Ohmiya, S.; Yoshimura, T.; Saitoh, T. Resistance spot welding of steel and aluminium sheet using insert metal sheet. *Sci. Technol. Weld. Join.* **1999**, *4*, 80–88. [CrossRef]
54. Cui, L.H.; Qiu, R.F.; Shi, H.X.; Zhu, Y.M. Resistance Spot Welding between Copper Coated Steel and Aluminum Alloy. *Appl. Mech. Mater.* **2014**, *675–677*, 19–22. [CrossRef]
55. Triwanapong, S.; Kaewwichit, J.; Roybang, W.; Kimapong, K. Optimization of Friction Stir Spot Welding Parameters of Lap Joint between AA1100 Aluminum Alloy and SGACD Zinc-coated Steel. *Int. J. Adv. Cult. Technol.* **2015**, *3*, 161–168. [CrossRef]
56. Morsy, M.A.; El-Alim, H.A.; El-Kashif, E. Dissimilar Friction Stir Spot Welding of Aluminum, Steel, and Brass Alloys. *J. Eng. Appl. Sci.* **2010**, *57*, 149–165.
57. Zhang, W.H.; Qiu, X.M.; Sun, D.Q.; Han, L.J. Effects of resistance spot welding parameters on microstructures and mechanical properties of dissimilar material joints of galvanised high strength steel and aluminium alloy. *Sci. Technol. Weld. Join.* **2011**, *16*, 153–161. [CrossRef]
58. Baek, S.; Song, J.; Lee, H.C.; Park, S.Y.; Song, K.H.; Lee, S.; Lee, S.J.; Chen, C.; Kim, D. Robust bonding and microstructure behavior of aluminum/high-strength steel lap joints using resistance element welding process for lightweight vehicles: Experimental and numerical investigation. *Mater. Sci. Eng. A* **2022**, *833*, 142378. [CrossRef]
59. Qiu, R.; Wang, N.; Shi, H.; Cui, L.; Hou, L.; Zhang, K. Joining steel to aluminum alloy by resistance spot welding with a rivet. *Int. J. Mater. Res.* **2015**, *106*, 60–65. [CrossRef]
60. Fei, L.; Zhao, S.; Zhang, P.; Feng, Z.; Jiang, F.; Zhou, H. Microstructure and mechanical performance of flat resistance element welded aluminum alloy/Q235 steel joints. *Int. J. Adv. Manuf. Technol.* **2022**, *120*, 6337–6349. [CrossRef]
61. Niu, S.; Lou, M.; Ma, Y.; Li, Y. Study on the microstructure and mechanical performance for integrated resistance element welded aluminum alloy/press hardened steel joints. *Mater. Sci. Eng. A* **2021**, *800*, 140329. [CrossRef]
62. Günter, H.; Meschut, G. Joining of ultra-high-strength steels using resistance element welding on conventional resistance spot welding guns. *Weld. World* **2021**, *65*, 1899–1914. [CrossRef]
63. Meschut, G.; Janzen, V.; Olfermann, T. Innovative and highly productive joining technologies for multi-material lightweight car body structures. *J. Mater. Eng. Perform.* **2014**, *23*, 1515–1523. [CrossRef]
64. Niu, S.; Ma, Y.; Lou, M.; Zhang, C.; Li, Y. Joint formation mechanism and performance of resistance rivet welding (RRW) for aluminum alloy and press hardened steel. *J. Mater. Process. Technol.* **2020**, *286*, 116830. [CrossRef]
65. Williams, N.T.; Parker, J.D. Review of resistance spot welding of steel sheets: Part 1—Modelling and control of weld nugget formation. *Int. Mater. Rev.* **2004**, *49*, 45–75. [CrossRef]
66. Manladan, S.M.; Yusof, F.; Ramesh, S.; Fadzil, M.; Luo, Z.; Ao, S. A review on resistance spot welding of aluminum alloys. *Int. J. Adv. Manuf. Technol.* **2017**, *90*, 605–634. [CrossRef]
67. Wang, Y.R.; Mo, Z.H.; Feng, J.C.; Zhang, Z.D. Effect of welding time on microstructure and tensile shear load in resistance spot welded joints of AZ31 Mg alloy. *Sci. Technol. Weld. Join.* **2013**, *12*, 671–676. [CrossRef]
68. Pereira, A.M.; Ferreira, J.M.; Loureiro, A.; Costa, J.D.M.; Bártolo, P.J. Effect of process parameters on the strength of resistance spot welds in 6082-T6 aluminium alloy. *Mater. Des.* **2010**, *5*, 2454–2463. [CrossRef]
69. Florea, R.S.; Bammann, D.J.; Yeldell, A.; Solanki, K.N.; Hammi, Y. Welding parameters influence on fatigue life and microstructure in resistance spot welding of 6061-T6 aluminum alloy. *Mater. Des.* **2013**, *45*, 456–465. [CrossRef]
70. Li, Y.; Luo, Z.; Yan, F.; Duan, R.; Yao, Q. Effect of external magnetic field on resistance spot welds of aluminum alloy. *Mater. Des.* **2014**, *56*, 1025–1033. [CrossRef]
71. De, A. Finite element modelling of resistance spot welding of aluminium with spherical tip electrodes. *Sci. Technol. Weld. Join.* **2002**, *7*, 119–124. [CrossRef]
72. Meschut, G.; Schmal, C.; Olfermann, T. Process characteristics and load-bearing capacities of joints welded with elements for the application in multi-material design. *Weld. World* **2017**, *61*, 435–442. [CrossRef]
73. Crinon, E.; Evans, J.T. The effect of surface roughness, oxide film thickness and interfacial sliding on the electrical contact resistance of aluminium. *Mater. Sci. Eng. A Struct. Mater.* **1998**, *242*, 121–128. [CrossRef]
74. Rashid, M.; Medley, J.B.; Zhou, Y. Nugget formation and growth during resistance spot welding of aluminium alloy 5182. *Can. Metall. Q.* **2011**, *50*, 61–71. [CrossRef]
75. Miyamoto, K.; Nakagawa, S.; Sugi, C.; Sakurai, H.; Hirose, A. Dissimilar joining of aluminum alloy and steel by resistance spot welding. *SAE Tech. Pap.* **2009**, *2*, 58–67. [CrossRef]
76. Abdul Karim, M.; Park, Y.-D. A Review on Welding of Dissimilar Metals in Car Body Manufacturing. *J. Weld. Join.* **2020**, *38*, 8–23. [CrossRef]

77. Ji, C.W.; Jo, I.; Lee, H.; Choi, I.D.; Do Kim, Y.; Park, Y.D. Effects of surface coating on weld growth of resistance spot-welded hot-stamped boron steels. *J. Mech. Sci. Technol.* **2014**, *28*, 4761–4769. [CrossRef]
78. Meinhardt, M.; Lechner, M.; Merklein, M. Experimental analysis of the influence of the embossing and upsetting process on joint strength in resistance element welding with upset auxiliary joining elements. *IOP Conf. Ser. Mater. Sci. Eng.* **2021**, *1157*, 012002. [CrossRef]
79. Wang, S.; Li, Y.; Yang, Y.; Manladan, S.M.; Luo, Z. Resistance element welding of 7075 aluminum alloy to Ti6Al4V titanium alloy. *J. Manuf. Process.* **2021**, *70*, 300–306. [CrossRef]
80. Qiu, R.; Shi, H.; Zhang, K.; Tu, Y.; Iwamoto, C.; Satonaka, S. Interfacial characterization of joint between mild steel and aluminum alloy welded by resistance spot welding. *Mater. Charact.* **2010**, *61*, 684–688. [CrossRef]
81. Manladan, S.M.; Zhang, Y.; Ramesh, S.; Cai, Y.; Ao, S.; Luo, Z. Resistance element welding of magnesium alloy and austenitic stainless steel in three-sheet configurations. *J. Mater. Process. Technol.* **2019**, *274*, 116292. [CrossRef]
82. Zhang, H.; Senkara, J. *Resistance Welding: Fundamentals and Applications*, 2nd ed.; CRC Press: Boca Raton, FL, USA, 2011. [CrossRef]
83. Wang, Y.R.; Feng, J.C.; Zhang, Z.D. Microstructure characteristics of resistance spot welds of AZ31 Mg alloy. *Sci. Technol. Weld. Join.* **2013**, *11*, 555–560. [CrossRef]
84. AWS Bookstore. AWS D1.1/D1.1M: 2010 STRUCTURAL WELDING CODE-STEEL (AWS D1.1 File Has Been Released by AWS. The Books Are in Production at the Printers and Available for Shipment July 1st). Available online: https://pubs.aws.org/p/873/d11d11m2010-2nd-printing-structural-welding-code-steel-historical (accessed on 16 May 2024).
85. Chipman, J. Thermodynamics and phase diagram of the Fe-C system. *Metall. Trans.* **1972**, *3*, 55–64. [CrossRef]
86. Zhang, H.; Wei, A.; Qiu, X.; Chen, J. Microstructure and mechanical properties of resistance spot welded dissimilar thickness DP780/DP600 dual-phase steel joints. *Mater. Des.* **2014**, *54*, 443–449. [CrossRef]
87. Pouranvari, M.; Marashi, S.P.H. Failure mode transition in AHSS resistance spot welds. Part I. Controlling factors. *Mater. Sci. Eng. A* **2011**, *528*, 8337–8343. [CrossRef]
88. Liu, L.; Ren, D.; Li, Y. Static mechanics analyses of different laser weld bonding structures in joining AZ61 Mg alloy. *Int. J. Adhes. Adhes.* **2011**, *31*, 660–665. [CrossRef]
89. Carboni, M.; Moroni, F. Tensile-Shear Fatigue Behavior of Aluminum and Magnesium Lap-Joints obtained by Ultrasonic Welding and Adhesive Bonding. *Procedia Eng.* **2011**, *10*, 3561–3566. [CrossRef]
90. Zhang, W.; Sun, D.; Han, L.; Li, Y. Optimised design of electrode morphology for novel dissimilar resistance spot welding of aluminium alloy and galvanised high strength steel. *Mater. Des.* **2015**, *85*, 461–470. [CrossRef]
91. Dong, H.; Hu, W.; Duan, Y.; Wang, X.; Dong, C. Dissimilar metal joining of aluminum alloy to galvanized steel with Al-Si, Al-Cu, Al-Si-Cu and Zn-Al filler wires. *J. Mater. Process. Technol.* **2012**, *212*, 458–464. [CrossRef]
92. Zhang, W.; Sun, D.; Han, L.; Liu, D. Interfacial microstructure and mechanical property of resistance spot welded joint of high strength steel and aluminium alloy with 4047 AlSi12 interlayer. *Mater. Des.* **2014**, *57*, 186–194. [CrossRef]
93. Arghavani, M.R.; Movahedi, M.; Kokabi, A.H. Role of zinc layer in resistance spot welding of aluminium to steel. *Mater. Des.* **2016**, *102*, 106–114. [CrossRef]
94. Fei, L.; Zhao, S.; Zhang, P.; Feng, Z.; Jiang, F.; Zhang, Y. Study on the microstructure and failure mechanisms for flat resistance element welding-bonding aluminium alloy/Q235 steel joints. *Sci. Technol. Weld. Join.* **2023**, *28*, 63–71. [CrossRef]
95. Bartczak, B.; Mucha, J.; Trzepieciński, T. Stress distribution in adhesively-bonded joints and the loading capacity of hybrid joints of car body steels for the automotive industry. *Int. J. Adhes. Adhes.* **2013**, *45*, 42–52. [CrossRef]
96. Schmal, C.; Meschut, G. Process characteristics and influences of production-related disturbances in resistance element welding of hybrid materials with steel cover sheets and polymer core. *Weld. World* **2020**, *64*, 437–448. [CrossRef]
97. Troschitz, J.; Vorderbrüggen, J.; Kupfer, R.; Gude, M.; Meschut, G. Joining of Thermoplastic Composites with Metals Using Resistance Element Welding. *Appl. Sci.* **2020**, *10*, 7251. [CrossRef]
98. Wu, S.N.; Ghaffari, B.; Hetrick, E.; Li, M.; Jia, Z.H.; Liu, Q. Microstructure characterization and quasi-static failure behavior of resistance spot welds of AA6111-T4 aluminum alloy. *Trans. Nonferrous Met. Soc. China (Engl. Ed.)* **2014**, *24*, 3879–3885. [CrossRef]
99. Sun, X.; Stephens, E.V.; Davies, R.W.; Khaleel, M.A.; Spinella, D.J. Effects of Fusion Zone Size on Failure Modes and Static Strength of Aluminum Resistance Spot Welds. *Weld. J.* **2004**, *83*, 308s–318s.
100. Florea, R.S.; Solanki, K.N.; Bammann, D.J.; Baird, J.C.; Jordon, J.B.; Castanier, M.P. Resistance spot welding of 6061-T6 aluminum: Failure loads and deformation. *Mater. Des.* **2012**, *34*, 624–630. [CrossRef]
101. ASM International. Fatigue and fracture. In *ASM Handbook*; ASM International: Materials Park, OH, USA, 1996; Volume 19, p. 1057.
102. Zhu, S.P.; Ye, W.L.; Correia, J.A.F.O.; Jesus, A.M.P.; Wang, Q. Stress gradient effect in metal fatigue: Review and solutions. *Theor. Appl. Fract. Mech.* **2022**, *121*, 103513. [CrossRef]
103. Bjørheim, F.; Siriwardane, S.C.; Pavlou, D. A review of fatigue damage detection and measurement techniques. *Int. J. Fatigue* **2022**, *154*, 106556. [CrossRef]
104. Malekinejad, H.; Carbas, R.J.C.; Akhavan-Safar, A.; Marques, E.A.S.; Castro Sousa, F.; da Silva, L.F.M. Enhancing Fatigue Life and Strength of Adhesively Bonded Composite Joints: A Comprehensive Review. *Materials* **2023**, *16*, 6468. [CrossRef] [PubMed]
105. Sousa, F.C.; Zamani, P.; Akhavan-Safar, A.; da Silva, L.F.M. A comprehensive review of the S-N fatigue behaviour of adhesive joints. *J. Adv. Join. Process.* **2024**, *9*, 100178. [CrossRef]

106. Hassanifard, S.; Zehsaz, M.; Tohgo, K. The effects of electrode force on the mechanical behaviour of resistance spot-welded 5083-o aluminium alloy joints. *Strain* **2011**, *47*, e196–e204. [CrossRef]
107. Shi, Y.; Guo, H. Fatigue performance and fatigue damage parameter estimation of spot welded joints of aluminium alloys 6111-T4 and 5754. *Fatigue Fract. Eng. Mater. Struct.* **2013**, *36*, 1081–1090. [CrossRef]
108. Rao, H.M.; Kang, J.; Shi, L.; Sigler, D.R.; Carlson, B.E. Effect of specimen configuration on fatigue properties of dissimilar aluminum to steel resistance spot welds. *Int. J. Fatigue* **2018**, *116*, 13–21. [CrossRef]
109. Uematsu, Y.; Tokaji, K.; Tozaki, Y.; Nakashimac, Y. Fatigue behaviour of dissimilar friction stir spot weld between A6061 and SPCC welded by a scrolled groove shoulder tool. *Procedia Eng.* **2010**, *2*, 193–201. [CrossRef]
110. Okane, M.; Shitaka, T.; Ishida, M.; Chaki, T.; Yasui, T.; Fukumoto, M. Fatigue Properties of Butt Welded Aluminum Alloy and Carbon Steel Joints by Friction Stirring. *J. Phys. Conf. Ser.* **2017**, *843*, 012040. [CrossRef]
111. Pouranvari, M.; Marashi, S.P.H.; Safanama, D.S. Failure mode transition in AHSS resistance spot welds. Part II: Experimental investigation and model validation. *Mater. Sci. Eng. A* **2011**, *528*, 8344–8352. [CrossRef]
112. Cahoon, J.R. An improved equation relating hardness to ultimate strength. *Metall. Trans.* **1972**, *3*, 3040. [CrossRef]
113. *EN 1993-1-8:2005*; Eurocode 3: Design of Steel Structures—Part 1-8: Design of Joints. European Committee for Standardization: Brussels, Belgium, 2005.
114. Rao, Z.; Liu, L.; Wang, Y.; Ou, L.; Liu, J. Preventing nugget shifting in joining of dissimilar steels via resistance element welding: A numerical simulation. *Int. J. Adv. Manuf. Technol.* **2021**, *117*, 227–241. [CrossRef]
115. Zhang, W.; Xu, J. Advanced lightweight materials for Automobiles: A review. *Mater. Des.* **2022**, *221*, 110994. [CrossRef]
116. Siddesh Kumar, N.M.; Dhruthi Pramod, G.K.; Samrat, P.; Sadashiva, M. A Critical Review on Heat Treatment of Aluminium Alloys. *Mater. Today Proc.* **2022**, *58*, 71–79. [CrossRef]
117. Park, H.G.; Kumar, D.; Park, K.S.; Nam, K.S.; Kim, Y.; Kim, Y.M.; Lee, T. Electrode life evaluation for varied electrode material composition and geometry in resistance spot welding of aluminum alloys. *Weld. World* **2024**, *68*, 2701–2712. [CrossRef]
118. Zhao, D.; Vdonin, N.; Bezgans, Y.; Radionova, L.; Glebov, L. Correlating Electrode Degradation with Weldability of Galvanized BH 220 Steel during the Electrode Failure Process of Resistance Spot Welding. *Crystals* **2023**, *13*, 39. [CrossRef]
119. Panza, L.; Maddis MDe Spena, P.R. Use of electrode displacement signals for electrode degradation assessment in resistance spot welding. *J. Manuf. Process.* **2022**, *76*, 93–105. [CrossRef]
120. Panza, L.; Bruno, G.; Antal, G.; De Maddis, M.; Russo Spena, P. Machine learning tool for the prediction of electrode wear effect on the quality of resistance spot welds. *Int. J. Interact. Des. Manuf.* **2024**, *18*, 4629–4646. [CrossRef]
121. Zhang, X.; Ma, Y.; Li, W.; Huang, W.; Zhang, W.; Wang, Z.H. A review of residual stress effects on fatigue properties of friction stir welds. *Crit. Rev. Solid State Mater. Sci.* **2023**, *48*, 775–813. [CrossRef]
122. Tabatabaeian, A.; Ghasemi, A.R.; Shokrieh, M.M.; Marzbanrad, B.; Baraheni, M.; Fotouhi, M. Residual Stress in Engineering Materials: A Review. *Adv. Eng. Mater.* **2022**, *24*, 2100786. [CrossRef]